Atmospheric
Chemistry
and Physics
Discussions

Understanding the influence of combustion on atmospheric CO_2 over Europe by using satellite observations of CO_2 and reactive trace gases

Mehliyar Sadiq[1], Paul I. Palmer[1,2], Mark F. Lunt[1], Liang Feng[1,2], Ingrid Super[3], Stijn N. C. Dellaert[3], and Hugo A. C. Denier van der Gon[3]

[1]School of GeoSciences, University of Edinburgh, Edinburgh, UK
[2]National Centre for Earth Observation, University of Edinburgh, Edinburgh, UK
[3]Department of Climate, Air and Sustainability, TNO, P.O. Box 80015, 3508 TA Utrecht, the Netherlands

Correspondence: Mehliyar Sadiq (m.sadiq@ed.ac.uk)

Abstract. We assess how nitrogen oxides (NO_x=NO+NO_2), carbon monoxide (CO) and formaldehyde (HCHO) can be used as proxies to determine the combustion contribution to atmospheric carbon dioxide (CO_2) using satellite observations. We focus our analysis on 2018 when there is a full complement of column data from the TROPOspheric Monitoring Instrument (NO_2, CO, and HCHO) and the Orbiting Carbon Observatory-2 (CO_2). We use the nested GEOS-Chem atmospheric chemistry model to relate high-resolution emission inventories over Europe to these atmospheric data, taking into account scene-dependent averaging kernels. We find that that NO_2 and CO are the better candidates to identify incomplete combustion and fingerprints of different combustion sectors, but both have their own challenges associated with properly describing their atmospheric chemistry. The secondary source of HCHO from oxidation of biogenic volatile organic compounds, particularly over southern European countries, compromises its use as a proxy for combustion emissions. We find a weak positive correlation between the CO:CO_2 inventory ratio and observed column enhancements of ΔCO:ΔCO_2 (R<0.2), suggesting some consistency and linearity in CO chemistry and transport. However, we find a stronger negative correlation between the NO_x:CO_2 inventory ratio and observed column enhancements of ΔNO_2:ΔCO_2 (R<0.5), driven by non-linear photochemistry. Both of these observed ratios are described well by the GEOS-Chem atmospheric chemistry transport model, providing confidence of the quality of the emission inventory and that the model is a useful tool for interpreting these tracer-tracer ratios. Our results also provide some confidence in our ability to develop a robust method to infer combustion CO_2 emission estimates using satellite observations of reactive trace gases that have up until now mostly been used to study surface air quality.

1 Introduction

Mitigating the worst effects of future climate relies on our ability to reduce rapidly increasing atmospheric levels of gases emitted by human activities that effectively absorb outgoing infra-red radiation, and subsequently influence the warming of Earth's surface. Atmospheric carbon dioxide (CO_2) is the predominant trace gas that continues to affect Earth's contemporary global climate. Inventories of CO_2 that describe human activities, primarily derived from national-scale information about fuel

combustion and the amount of CO_2 released per unit of fuel burned, provide invaluable information the spatial and sectoral emission distributions. Assumptions embedded in the nationally-reported data and consequently the inventories can sometimes result in substantial uncertainties in the reported emissions. A complementary and independent approach to estimate CO_2

25 emissions is to use atmospheric CO_2 data that reflect the net cumulative result of emissions, atmospheric transport, and surface uptake. Quantifying the influence of fresh emissions on atmospheric CO_2 is an ongoing and pressing science objective. Here, we explore the relationships between CO_2 and reactive trace gases, co-emitted with CO_2 during combustion processes, to help isolate the combustion CO_2 from the biospheric fluxes.

Carbon-based fuels have historically dominated global energy use. Extracting energy from these fuels relies on breaking

30 apart atomic bonds that form the molecular structure of the fuel, thereby releasing energy. This is achieved by combustion in which the fuel, composed primarily of hydrogen-carbon bonds, is oxidized by molecular oxygen (O_2). Generally, more energy can be released during combustion for fuels with a higher H:C ratio. The primary combustion products are CO_2 and water vapour, but as the combustion becomes more inefficient (e.g. insufficient O_2 to react completely with the fuel) a wider range of compounds are released, determined by the composition of the fuel being burned. For many combustion processes, air is

35 used to provide O_2. While molecular nitrogen (N_2) in air does not take part in the combustion reaction, the high temperatures involved can thermally dissociate N_2 to facilitate the production of NO (and to a lesser extent NO_2) subject to the availability of O_2. Carbon monoxide (CO) is therefore a proxy for incomplete combustion of carbon-based fuel while the amount of NO_x ($NO+NO_2$) released during combustion is also associated with the combustion temperature.

Recent work has highlighted that biofuel combustion can represent a significant fraction of fuel burned over Europe, typically

40 10% for cities and power plants over western and southern Europe but up to 50% over Nordic cities that use more biomass for domestic heating (Ciais et al., 2020). However, as discussed later, we do not distinguish between combustion of fossil fuel and biofuel, instead focusing on isolating the combustion contribution to CO_2. We also do not attempt to determine emissions from individual sectors, which is currently limited by the data density of atmospheric CO_2 and co-emitted trace gases released by specific combustion processes.

45 The impetus for our study is the burgeoning capacity to observe accurately gradients of atmospheric CO_2 using satellites and to attribute those signals to specific regional fluxes. To separate the combustion emission portion of that signal, a growing number of studies have used NO_2 as a proxy for fossil fuel combustion to help infer CO_2 emissions (Reuter et al., 2019; Liu et al., 2020; Hakkarainen et al., 2021; Ialongo et al., 2021) while others have demonstrated current capabilities to infer emissions of NO_x, e.g., Fortems-Cheiney et al. (2021a, b), that can be used to develop *post hoc* estimates of CO_2 via sector-

50 based emission factors. The main advantage of using NO_2 as a tracer of combustion is its atmospheric e-folding lifetime, which ranges from hours to a day in the lower troposphere. Consequently, any major surface emissions will result in an observable plume close to the point of emission. The other advantage of using NO_2 is that it is observed by a range of current satellite instruments, although independent of current instruments observing CO_2. More importantly, CO_2 and NO_2 will be observed by the same instruments in the near future, including the Copernicus CO_2 Monitoring (CO2M) mission (Kuhlmann et al.,

55 2021) and the Japanese Greenhouse Gases Observing Satellite Greenhouse gases and Water cycle (GOSAT-GW). The value of using satellite column observations of NO_2 as a global tracer of anthropogenic CO_2 emissions has recently been outlined by

Finch et al. (2021) who used a deep learning method to identify every NO_2 plumes observed by the TROPOspheric Monitoring Instrument (TROPOMI) over a two-year period. They showed these plumes effectively mapped out most of the expected hotspots across the world, including large urban centres, oil and gas production, major power plants, and shipping routes.

60   Researchers have used CO as a proxy for incomplete combustion, e.g. (Kasibhatla et al., 2002; Palmer et al., 2006; Wang et al., 2009; Konovalov et al., 2014, 2016), which has similar advantages to using NO_2 but has a longer e-folding lifetime (weeks to months depending on season and latitude) and a large, seasonally varying secondary source from the oxidation of volatile organic compounds (VOCs). Some of these shortcomings will be overcome as measurements progressively have the capability to resolve smaller spatial scales that are closer to the scale of the responsible point sources. Formaldehyde (HCHO)
65   is another proxy for incomplete combustion (e.g., Fu et al. (2007a); Gonzi et al. (2011)) but the secondary source of HCHO and its uncertainty from the oxidation of biogenic VOCs, particularly over southern Europe (Curci et al., 2010), is sufficiently large to compromise this measurement from being used effectively to isolate combustion.

Recent studies have used satellite observations and emission inventories to analyze enhancements of atmospheric CO_2 and co-emitted species (CO and NO_x) over individual megacities (Hakkarainen et al., 2019; Berezin et al., 2013; Silva et al., 2013)
70   and large urban areas (Silva and Arellano, 2017; Labzovskii et al., 2019; Lama et al., 2020; Park et al., 2021) but have not critically assessed the efficacy of using these data together to isolate the combustion contribution to CO_2, which will eventually be needed to support more formal Bayesian inference methods. In this study, we explore the agreement between model and observed ratios of NO_2, CO, and HCHO with CO_2 by taking advantage of a new, high-resolution self-consistent European emission inventory for these gases (Super et al., 2020), a high-resolution chemistry transport model centred over Europe, and
75   co-located satellite column measurements of CO_2, NO_2, CO, and HCHO. We combine this information to interpret model and observed ratios at the model grid-scale resolution and at the national scale over Europe.

In the next section, we describe the nested version of GEOS-Chem that we use to study the relationships between emissions and corresponding atmospheric ratios of CO_2 and NO_2 and CO over Europe. We also describe the satellite data we use to evaluate these model relationships. In Sect. 3 we present our analysis and critically assess the efficacy of these ratios to isolate
80   the combustion contribution of CO_2. We conclude the paper in Sect. 4.

2   Data and Methods

Here we describe the nested GEOS-Chem atmospheric chemistry transport model and the satellite data we use to explore the relationships between CO_2, NO_2, and CO. For the purposes of this study, we focus on contrasting summer (July) and winter (December) months during 2018 when there are data from all relevant satellite instruments.

85   ### 2.1   GEOS-Chem atmospheric chemistry transport model

We use v12.6.1 of the GEOS-Chem 3-D atmospheric chemistry transport model (www.geos-chem.org) to describe the relationship between surface fluxes and atmospheric concentrations of CO, NO_2, and CO_2. We drive the GEOS-Chem model with

Goddard Earth Observing System, forward processing (GEOS-FP) meteorological analyses from the Global Modeling and Assimilation Office (GMAO) at NASA Goddard Space Flight Center.

90 For the experiments presented here, we use the nested version of GEOS-Chem to study atmospheric CO, NO_2, and CO_2 over Europe (broadly defined as 15° W–40° E, 30°–70° N, taking into account a buffer zone that helps to absorb any discontinuities associated with the coarser lateral boundary conditions), driven by the GEOS-FP meteorological analysis at its native spatial resolution of 0.25° (latitude) × 0.3125° (longitude). To provide time-dependent lateral boundary conditions for the nested model, we use a self-consistent version of GEOS-Chem at a coarser resolution of 4° (latitude) × 5° (longitude). For both

95 models we use 47 hybrid-sigma levels from the surface to 0.01 hPa, of which 30 lie below the dynamical troposphere.

We use a GEOS-Chem simulation that includes HO_x-NO_x-VOC-ozone-halogen-aerosol tropospheric chemistry, which is coupled with stratospheric chemistry via the unified tropospheric-stratospheric Chemistry eXtension (Eastham et al., 2014). For our global run, we use anthropogenic emissions of chemically reactive gases (CO, CH_4, NH_3, NO_x, SO_2, non-methane volative organic compounds (VOCs)), carbonaceous aerosols (including black carbon and organic carbon), and CO_2, from the

100 Community Emission Data System (CEDS) global emission inventory (Hoesly et al., 2018). Offline dust aerosol, lightning and soil NO_x, biogenic VOCs and sea salt aerosols emissions (Weng et al., 2020) are used in both global and regional simulations. We use Global Fire Emissions Database version 4 (GFED4, http://globalfiredata.org) to describe pyrogenic emissions. The GFED inventory provides monthly dry matter emissions based on satellite observations of fire activity and vegetation coverage from MODIS (Moderate Resolution Imaging Spectroradiometer, van Marle et al. (2017)). The GEOS-Chem model calculates

105 biomass burning emissions of trace gases and aerosols by applying vegetation-specific emission factors (Akagi et al., 2011) to the dry matter burned data.

For our nested European domain, we replace our global inventory anthropogenic emissions of CO, NO_x, CO_2 with the TNO-GHGco inventory (Netherlands Organization for Applied Scientific Research (TNO), greenhouse gas and co-emitted species emission database, Super et al. (2020)). This inventory is based on national emissions submitted to the United Nations

110 Framework Convention on Climate Change for CO_2 and to the European Monitoring and Evaluation Programme/Centre on Emission Inventories and Projections for NO_x and CO. National totals are distributed across individual countries on a 0.05° latitude × 0.1° longitude grid by using proxies such as the location of large industrial point sources, industrial area land cover maps for industrial emissions, and road networks derived from Open street map and Open transport map for road transport emissions (Super et al., 2020). Annual emissions are distributed in time using temporal emission profiles according to month,

115 day of the week, and the hour of day for every GNFR (Gridded Nomenclature For Reporting) sector code, based on the sector specific emission data reported by each country, and long-term mean activity data and/or socio-economic characteristics. The TNO-GHGco inventory includes 16 sectors (code - sector): A - Public Power, B - Industry, C - Other Stationary Combustion, D - Figutives, E - Solvents, F - Road Transport (F1–F4), G - Shipping, H - Aviation, I - Off-road transport, J - Waste, K - Agriculture Live Stock and L - Agriculture Others. The TNO-GHGco inventory also separates fossil fuel and biofuel emissions of CO_2 and

120 CO. Emissions of NO_x are converted to units of kg NO_2 m^{-2} s^{-1} for both the global (CEDS) and the regional (TNO-GHGco) inventories, and used as such in the GEOS-Chem model simulations. Consequently, we report NO_x emissions in the same units. We combine emissions from ten GNFR sectors (public power, industry, other stationary combustion, fugitives, all three

types of road transport, shipping, aviation and off road transport) that involve the combustion of fossil fuel and biofuel to form combustion emissions. This step is in recognition that we cannot separate emissions from different sectors or the combustion

125 of two fuel types, in terms of their contribution to observed atmospheric CO_2 and NO_2 columns.

Figure 1 shows the European distribution of TNO-GHGco combustion emission estimates (kg m^{-2} s^{-1}) of CO_2, NO_x, and CO for July and December 2018. Combustion emissions are high over major cities (e.g., London, Paris, Madrid), industrial areas, and over major land and ocean transportation networks, as expected. Figure 2 shows monthly sector contributions to national total combustion emissions of CO_2, NO_x, and CO during July and December 2018 from the six highest emitting

130 European countries, including the United Kingdom. In general, differences in the spatial distributions of emissions (Fig. 1) of these three trace gases and between July and December reflect the relative national importance of individual sectors (Fig. 2) that contribute to our combustion emission. Combustion emissions during December are generally higher than July, due primarily to a contribution from residential heating (C: Other Stationary Combustion) during the colder month (Fig. 2). We find that the six top CO_2 emitting countries for these three gases are consistently Germany, United Kingdom, France, Italy,

135 Poland, and Spain. Germany is the largest emitter of NO_x, CO, and CO_2, except for CO during December 2018. The largest contributing sectors for these top CO_2 emitting countries for NO_x, CO, and CO_2 are usually public power, industry, residential heating and transportation (Fig. A1). In terms of fuel type, the majority of CO_2 emissions comes from fossil fuel combustion in both July and December for the top 14 CO_2 emitting countries in the domain (Fig. A2), while for CO more than 50% of the emissions during December comes from biofuel combustion for France, Italy, Spain, Austria, Sweden and Portugal (Fig. A3).

140 **2.2 Satellite observations of CO_2, NO_2, and CO**

We use dry-air column CO_2 (XCO_2) observations retrieved by the NASA Orbiting Carbon Observatory-2 (OCO-2), launched in July 2014 into a sun-synchronous orbit with a local equatorial crossing time of 13:30 in its ascending node (Eldering et al., 2017). The dimensions of the ground footprint of XCO_2 is nominally 1.25 km across track and ≃2.4 km along track, determined by the instrument field of view, the orbital speed of the satellite, and the measurement integration time. OCO-2 includes three

145 spectrometers that measure two CO_2 bands (1.61 and 2.06 μm) and the O_2 A-Band (0.765 μm) (Crisp et al., 2004). For this study, we use OCO-2 Version 10 "Lite" (v10r) data, which is a bias-corrected and quality filtered Level 2 XCO_2 retrievals. First, the bias correction procedure maps the raw XCO_2 retrievals of the OCO-2 Level 2 algorithm to the best available estimate of XCO_2, using multi-model mean and TCCON measurements as training data sets (O'dell et al., 2018). Then, additional outlier filtering is applied to screen out low quality data based on parameters such as albedo, aerosol optical depth and cloud fraction

150 (Crisp et al., 2021). On monthly timescales, 7 to 12 % of these measurements are considered clear-sky data (cloud and aerosol free) that pass all quality tests, with single measurement random errors between 0.5 and 1 ppm at solar zenith angles smaller than 70° (Eldering et al., 2017).

We also use satellite column observations of CO, NO_2, and HCHO from the TROPOMI, aboard the European Space Agency's Sentinel-5 Precursor satellite. TROPOMI satellite was launched in 2017 into a sun-synchronous orbit with a local

155 equatorial overpass time of 13:30 in its ascending node. TROPOMI is a nadir viewing instrument that contains four spectrometers that cover UV-Vis-NIR-SWIR wavelengths. With a cross-track swath of 2600 km and a high spatial ground footprint

resolution of 7×7 km^2, TROPOMI has near-daily global coverage, subject to cloud-free scenes (Veefkind et al., 2012). Its operational level 2 trace gas data products include NO_2, CO, CH_4, O_3, HCHO, and SO_2). For the purposes of brevity, we refer the reader to dedicated studies that describe the retrieval of CO (Vidot et al., 2012; Landgraf et al., 2016), NO_2 (Boersma
160   et al., 2010; Van Geffen et al., 2015; Lorente et al., 2017; Zara et al., 2018; Van Geffen et al., 2020), and HCHO (Platt and Stutz, 2008; Smedt et al., 2018). Tropospheric column retrieval biases of CO, NO_2, and HCHO are <10%, 25–50%, and 80%, respectively. We use TROPOMI satellite retrievals that have a quality assurance flag with a value >0.5 for CO, >0.75 for NO_2 and >0.5 for HCHO, which removes cloud-covered scenes, partially snow/ice covered scenes, errors and problematic retrievals, as recommended by respective technical descriptions (https://sentinels.copernicus.eu/web/sentinel/technical-guides/
165   sentinel-5p/products-algorithms, last accessed 14th July 2021)

3   Results

Here we report our analysis of TNO-GHGco emissions estimates of CO, NO_x, and CO_2 and their ratios, and the corresponding model atmospheric column concentrations and their ratios, which we compare with observed values calculated from OCO-2 and TROPOMI. We do not consider emission ratios that include HCHO because the direct emission is small compared to the
170   contribution from methane and non-methane VOCs.

3.1   Inventory emission ratios of combustion NO_x:CO_2 and CO:CO_2

Figure 3 shows the inventory combustion emission ratios, described as mole fractions, of NO_x:CO_2 and CO:CO_2 during July and December 2018, corresponding to values shown in Fig. 1. These gridded ratios represent the net combustion efficiency of total emissions weighted by the influence of individual sectors. Generally, higher values of CO:CO_2 and NO_x:CO_2 denote a
175   lower combustion efficiency, with higher NO_x:CO_2 values also associated with higher combustion temperatures. We find that the NO_x:CO_2 ratio is higher in July than December, but CO:CO_2 ratio is generally higher in December than July, which is reflected in the national mean values (Fig. 4). This is due to a larger contribution from residential heating (C: Other Stationary Combustion) to net emissions during December (Fig. 2) for which NO_x:CO_2 values (0.49–1.95) are lower and CO:CO_2 values (0.60–4.25) are generally higher than for other sectors (Fig. 4).

180   Figure 4 shows a heatmap of combustion emission mole ratios from eight major sectors (A: Public Power, B: Industry, C: Other Stationary Combustion, F1: Road Transport Gasoline, F2: Road Transport Diesel, F3: Road Transport LPG Gas, G: Shipping and I: Off Road, two sectors excluded here are D: Fugitives and H: Aviation) in the top 14 CO_2 emitting countries (in descending order). We find NO_x:CO_2 values are higher in shipping, off-road transport and diesel road transport. CO:CO_2 values are generally higher in off-road transport, residential heating and gasoline road transport. These ratios are assumed to
185   be the same in different months of the year (Super et al., 2020), hence total combustion ratios in July and December only differ in the relative contribution from each sector (Fig. 2 and A1). In terms of NO_x:CO_2, Portugal, Norway and Spain are higher than neighbouring European countries, with Germany having the lowest value. In terms of CO:CO_2, Germany has a lower values than its neighbouring countries. The differences between countries for the two months reflect the relative importance of

Atmospheric
Chemistry
and Physics
Open Access
EGU
Discussions

individual sectors (Fig. 2, 4 and A1), in particular, the relative importance of transport, domestic heating and shipping emission.

190 Closer inspection of Fig. 1 reveals hotspots of CO_2 that correspond to cities, large point sources, and transport network. These CO_2 hotspots manifest themsleves as low values of the emission ratios (Fig. 3). Emissions in the marine troposphere are mainly due to ship exhaust, which emits more NO_x and less CO than land-based sectors, resulting in the rapid gradient of the ratios between land and ocean.

Figure 4 also shows the corresponding nationwide mean combustion emission ratios of $NO_x:CO_2$ and $CO:CO_2$ during July

195 and December 2018. Generally, $CO:CO_2$ ratios are higher than $NO_x:CO_2$ (note the different scaling factor), reflecting higher fossil fuel emission factors for CO than for NO_x. We find that national values of $NO_x:CO_2$ show a smaller dynamic range than corresponding values of $CO:CO_2$, particularly during July. This will have implications for using these ratios to determine combustion CO_2 emissions from individual countries, particularly those that are geographical neighbours. Portugal has the highest $NO_x:CO_2$ value in the domain, mostly determined by large industrial sources, shipping and off-road transportation.

200 Norway has the highest value for $CO:CO_2$, mostly contributed by emissions from large industries, residential heating and off-road transportation.

3.2 Comparison of observed and model column variations of CO_2, CO, NO_2 and HCHO

Figure A4 shows typical column averaging kernels for OCO-2 CO_2, and TROPOMI CO, NO_2, and HCHO, which describe the sensitivity of the retrieved columns to changes in these gases as a function of altitude through the atmosphere. Model

205 output, sampled at the time and location of each observation, is convolved with scene-dependent averaging kernels so it can be directly compared with observed columns. These averaging kernels generally show that the retrieved columns of all four gases are sensitive to varying degrees to changes in the lower troposphere where surface emissions have the largest impact on. Differences between the vertical sensitivities may result in the misinterpretation of the ratios that we attempt to avoid by applying the kernels to the model output.

210 ### 3.2.1 Satellite column observations

Figure 5a, b and c shows monthly OCO-2 CO_2, TROPOMI NO_2 and CO columns during July 2018, gridded on the GEOS-Chem nested model $0.25° \times 0.3125°$ grid. We find that NO_2 has the largest spatial variability across Europe, mainly reflecting its much shorter atmospheric lifetimes compared with CO and CO_2. Tropospheric NO_2 columns are generally elevated over major cities (e.g., London, Paris, Madrid), conurbations (e.g., Manchester, Liverpool) and industrial areas (e.g., Po Valley,

215 northern Italy) across Europe (Pope et al., 2018; Griffin et al., 2019; Finch et al., 2021). We do not consider December 2018 because the distribution of CO_2 used below to examine atmospheric trace gases ratios is too sparse due to cloudy scenes (Fig. A5).

Elevated columns of HCHO (Fig. A6) during July 2018 mainly reflect the oxidation of biogenic VOCs (Curci et al., 2010), particularly over southern European countries where Mediterranean vegetation are emitters of isoprene, which rapidly produces

220 HCHO with a large molar yield (Palmer et al., 2006; Surl et al., 2018). There are also small direct emissions and contributions from industrial activity via the oxidation of anthropogenic VOCs (e.g., Po Valley). The rate at which HCHO is produced from

the oxidation of anthropogenic VOCs tends to be much larger than biogenic VOCs so that the resulting HCHO column is smeared over neighbouring grid boxes (Palmer et al., 2003; Abbot et al., 2003; Fu et al., 2007b). Given the limited use of HCHO as a tracer of combustion we do not pursue this tracer any further.

225 In contrast to TROPOMI that has a wide cross-track swath, OCO-2 data are sparse that also reflects much stricter filtering criteria. With the exception of large point sources, the large, inhomogeneous and slowly varying background values of CO_2 precludes any meaningful attribution of elevated values to individual source regions without the use of an atmospheric transport model.

3.2.2 Satellite columns of CO_2, NO_2, and CO simulated by the GEOS-Chem model

230 We use the GEOS-Chem model (Sect. 2), driven by emission inventories (Sect. 2), to describe TROPOMI CO, NO_2, and OCO-2 CO_2. To compare model columns with observations, we first sample the model at the local time and location of each observation, map the modeled 3-D concentration field onto the satellite retrieval levels (20 for OCO-2 and 34 for TROPOMI), and then compute the modeled columns using scene-dependent averaging kernels. The GEOS-Chem model then become an intermediary that relates the TNO-GHGco emission inventories (Sect. 2) to the satellite observations.

235 For OCO-2 column CO_2, the equivalent model XCO_2^m is calculated using:

$$XCO_2{}^m = XCO_2{}^a + \sum_i \boldsymbol{\eta}_i \mathbf{a}_i (F(\mathbf{x}) - \mathbf{y}_{a,i}), \qquad (1)$$

where $F(\mathbf{x})$ denotes the GEOS-Chem model that relates *a priori* flux estimates $\mathbf{x}$ to a scene-dependent CO_2 profile and the log-linear interpolation of those values on the model pressure levels to i pressure levels used by the XCO_2 retrieval algorithm, which uses its own *a priori* values denoted by $\mathbf{y}_a$ (corresponding to the the column XCO_2^a). The pressure weighting function
240 $\boldsymbol{\eta}_i$ includes the pressure intervals assigned to the satellite retrieval levels, and $\mathbf{a}_i$ denotes the scene-dependent averaging kernel that describes the sensitivity of the instrument to CO_2 as a function of altitude (e.g., Fig. A4). For TROPOMI columns of CO and NO_2, we use a similar method to translate the model into observation space. For NO_2, we consider only the tropospheric column. A detailed description of the method is given by Van Geffen et al. (2020).

Figure 5 shows OCO-2 and TROPOMI measurements and GEOS-Chem model values for CO_2, CO and NO_2 during July
245 2018. The model generally reproduces well the observed monthly spatial variations for CO_2 ($R=0.67$), CO ($R=0.28$) and NO_2 ($R = 0.18$) across Europe, but has a relative bias of -0.33%, -14.6% and +50.8%, respectively. In addition to capturing the major NO_2 column hotspots, e.g., southern England, Belgium, Netherlands and northern Italy, Fig. 5 shows that elevated NO_2 columns are more widespread in GEOS-Chem than TROPOMI. Higher model values over land likely reflect over-reporting of NO_x emissions from rural areas of France, Germany, Poland and other eastern European countries, i.e., errors in emission
250 inventory, temporal profile and errors in vertical mixing and lifetime of NO_x against chemical oxidation. This positive model bias could also be due to the mismatch between emission timing and satellite overpass. Overestimation of NO_2 columns over the Bay of Biscay and the northern Mediterranean Sea reflect errors in the modelling of lightning (influencing the upper troposphere), vertical mixing over water, NO_x lifetime, over-reporting of NO_2 shipping emission, and challenges in detecting surface concentrations of NO_2 from shipping (Laughner et al., 2016) (Fig. 1). The lifetime of NO_x is of the order of hours and

Atmospheric
Chemistry
and Physics
Discussions
Open Access
EGU

255 changes with the chemical environment, including the NO_x concentration itself, e.g. Laughner and Cohen (2019). GEOS-Chem fails to capture the highest values in TROPOMI NO_2 columns, especially over London, Paris, Madrid, Belgium, Netherlands and western Germany, which is due to some combination of underestimating emissions from these large urban sources, errors in the model description of NO_x photochemistry, and the low sensitivity of averaging kernels to lower levels of the atmosphere (Fig. A4).

260 Figure 5 also shows there is better relative agreement between GEOS-Chem and TROPOMI for CO than for NO_2, with a mean percentage bias of -14.6% compared with 50.8% for NO_2, and a better spatial correlation. This reflects the longer atmospheric lifetime for CO (weeks during summertime) against oxidation by the hydroxyl radical so that atmospheric distributions are less influenced than NO_2 columns by immediate and local surface emissions. Observed variations of CO columns represent the sum of direct emissions from incomplete combustion and a secondary source from the oxidation of methane and

265 non-methane VOCs (Duncan et al., 2007). The secondary source is usually assumed to be a diffuse source of CO because of the time it typically takes to produce CO. Using GEOS-Chem, we find that the secondary source is typically 10–20% of the total CO source in winter months but in July can be as much as 75% of the total CO source over Europe. This secondary source will therefore need to be considered if CO is to be used to isolate combustion CO_2.

Large model bias for CO (negative) and NO_2 (positive), as reported above, limits our ability to infer directly combustion

270 CO_2 from these data. However, the reasonably high spatial correlation between GEOS-Chem and TROPOMI (R=0.60 for NO_2 and R=0.82 for CO) provide us with some confidence in our ability to use enhancement ratios of column CO and NO_2 (ΔNO_2 and ΔCO). To calculate these enhancements, we first determine latitude-dependent background values of the satellite data and then subtract those from the data. We calculate these background values (i.e., not directly influenced by urban enhancements) using monthly mean values over the remote Pacific Ocean (175° W to 165° W) in 10° latitude bins. Mean monthly observed

275 background levels of XCO_2, column NO_2 and column CO over the remote Pacific Ocean are 390 ppm, 2.46 μ mol m^{-2} and 20578 μ mol m^{-2}, respectively. We compute the corresponding background levels for GEOS-Chem model by adjusting the satellite observed background levels with the model bias (domain mean) in Fig. 5, assuming that model bias is mostly caused by the background level (boundary condition simulated by the global full chemistry simulation). We subtract these values from the observations and the GEOS-Chem model to determine ΔXCO_2, ΔXCO and ΔXNO_2. In the next section, we explore the

280 relationship between ΔNO_2 and ΔCO and the corresponding value of ΔCO_2.

3.3 Observed and model atmospheric variations of CO_2, NO_2, and CO columns

Figure 6 shows monthly means and the associated standard deviations of observed and model XCO_2, NO_2, and CO enhancements over Europe during July 2018 across the top 14 CO_2 emitting countries. During July 2018, observed XCO_2 enhancements over our European study domain have a mean enhancement of 14.8±1.86 ppm. Belgium, Spain and Portugal have the highest

285 XCO_2 enhancement values, but differences between countries and variations within each country are relatively small. Within our European study domain, observed column NO_2 and column CO enhancements have mean values of 52.3±33.6 pptv and 22.0±7.4 ppbv during July 2018, respectively. Countries with the highest column NO_2 enhancements are Belgium, Netherlands, Germany and UK, while differences in column CO enhancement between countries are relatively small. Model en-

hancements agree reasonably well with observed enhancements on national spatial scales (R=0.85 for CO_2, R=0.78 for NO_2,
290　R=0.96 for CO), except for column NO_2 enhancement in Netherlands, Belgium and Ireland (relative bias > 20%).

　　Figure 7 shows observed and model ΔXNO_2:ΔXCO_2 and ΔXCO:ΔXCO_2 ratios during July 2018. We find that observed monthly mean ΔXNO_2:ΔXCO_2 show higher values over Germany, Netherlands, Belgium, Northern Italy, UK and Poland, corresponding with the hotspots of NO_2 column measurements. The same ratios simulated by GEOS-Chem show high values over the same countries and France, Serbia, Romania and Bulgaria. We generally find that values of ΔXCO:ΔXCO_2 show
295　higher values over Eastern Europe than western European countries, both in observed and model values. These ratios are the atmospheric equivalent of the ratios determined by the emission inventory shown in Fig. 3. We find that model fails to capture ΔXNO_2:ΔXCO_2 hotspots such as Madrid and Paris due to failure to capture hotspots in column NO_2 concentration in Figure 5. To understand the relationship between the emissions and corresponding atmospheric values, we correlate the two sets of ratios at grid cell level and at national level for July 2018.

300　　　Figure 8a show the relationships between the national emissions ratios of CO:CO_2 and NO_x:CO_2 (Fig. 4) and the corresponding model and observed atmospheric ratios of ΔXCO:ΔXCO_2 and ΔXNO_2:ΔXCO_2. We find only a weak positive correlation (R=0.15) between the emission-based ratios, reflecting the importance of different sectors (with varying emission factors) within countries across Europe. Figure 8b shows observed and model national mean values for ΔXNO_2:ΔXCO_2 and ΔXCO:ΔXCO_2 ratios. We find that, on national level, both observed and model ratios are positively correlated, with correla-
305　tion coefficients of R=0.60 and R=0.66, respectively. This suggests both observed and model columns reproduce the positive relationship based on the inventory estimates. The comparatively strong correlations found for the observed and model atmospheric ratios reflect the atmospheric mixing of spatially heterogeneous emissions. Observed and model slopes from the linear regression of the the two ratios are 5.90 and 2.57 (unitless), respectively. Slope values reflect the co-enhancement of column NO_2 with CO, with the model having a smaller enhancement of NO_2 per unit of column CO enhancement. This suggests that
310　the inventory is in error and that the NO_x:CO should be smaller, and/or there is a larger NO_2 chemical loss than we describe in GEOS-Chem (or a smaller chemical loss of CO).

　　Figure 9 shows the model and observed relationship between the emission-based ratios of NO_x:CO_2 and CO:CO_2 and the corresponding atmospheric ratios of ΔXNO_2:ΔXCO_2 and ΔXCO:ΔXCO_2. Figures A7 and A8. show the grid-cell resolution analysis for the nine countries with the most amount of data. Figure 9 shows good agreement between model and measurements
315　in terms of the variation of the atmospheric ratio. The situation for the NO_2-based ratio (Fig. 9a) is more encouraging. Model and observed ΔXNO_2:ΔXCO_2 ratio are both negatively related to the inventory based NO_x:CO_2 ratio, with correlations of -0.69 for GEOS-Chem and -0.50 for the satellite observations. At the grid-scale resolution, the United Kingdom, Italy and Norway demonstrate the similar negative correlation. These countries do not differ significantly from other countries in terms of relative contribution from different sectors (Fig. 2 and Fig. A1), or national mean combustion ratios (Fig. 4). Hence, the negative
320　relationships between the inventory-based and atmospheric-based ratios reflect a strong non-linearity between NO_x emissions and NO_2 concentration. This is most likely due to NO_x photochemistry, since other factors are generally similar between our CO and NO_2 based ratios, e.g., meteorology. This strong negative correlation in NO_2 based ratios requires further investigation to understand how to best use this information to interpret combustion CO_2. Nevertheless, good (negative) correlations between

Atmospheric
Chemistry
and Physics
Discussions

emission-based ratios and the observed and model atmospheric column ratios could indicate the feasibility to infer combustion

325   CO_2 from satellite measurements and GEOS-Chem model using co-emitted CO and NO_x.

For CO (Fig. 9b), there is only a weak correlation between combustion $CO:CO_2$ and $\Delta XCO:\Delta XCO_2$ for both GEOS-Chem and the satellite observations, at national (Fig. 9) and at grid-cell resolutions (Fig. A8). Generally, we find there is more national variation between the inventory-based $CO:CO_2$ ratio than the corresponding atmospheric ratio, which is due to atmospheric mixing of CO that has an e-folding lifetime much longer than the transport time over Europe. Similar to the NO_2 based ratios,

330   GEOS-Chem overestimates the column enhancement ratio (Fig. 7b and d).

4   Concluding remarks

We assessed how three reactive trace gases, nitrogen dioxide (NO_2), carbon monoxide (CO) and formaldehyde (HCHO), can be used as proxies to determine the combustion contribution to atmospheric CO_2 in July and December, two contrasting months in terms of sector emissions and photochemical environment, in 2018. Our choice to focus on combustion emissions

335   reflects varying contributions of biofuel combustion to national CO_2 emission budgets across Europe. We use satellite column measurements of CO_2 from the NASA Orbiting Carbon Observatory (OCO-2) and satellite tropospheric column data products of CO, NO_2, and HCHO from the European TROPospheric Ozone-Monitoring Instrument (TROPOMI) aboard Sentinel-5P. We focus our analysis on 2018 when there is a full year of data from OCO-2 and TROPOMI. We use a nested atmospheric chemistry transport model (GEOS-Chem) driven by self-consistent combustion emissions of CO_2, nitrogen oxides (NO_x), CO,

340   and volatile organic compounds (VOCs) that are precursors to HCHO.

We found that HCHO as a tracer of incomplete combustion is compromised during the summer by biogenic VOC emissions, particularly over the Mediterranean, and during the winter when the lifetimes of parent anthropogenic VOCs are too long to relate elevated HCHO columns to anthropogenic activity. Based on our assessment, we conclude that HCHO is unlikely to play a substantive role in quantifying the combustion contribution to CO_2.

345   Combustion emission estimates for CO_2, CO and NO_x in July and December 2018 show different spatial distribution due to different dominating emission sectors for these trace gases and also in contrasting months, which resulted in spatial variation in $CO:CO_2$ and $NO_x:CO_2$. Hence, we find that NO_2 and CO are the better proxies for combustion, but both have their own challenges. When using satellite measured ΔXNO_2 and ΔXCO as a way to identify characteristic $\Delta X:\Delta XCO_2$ ratios (where $X = NO_2$ or CO and Δ denotes elevated values above a regional background value) that correspond to combustion, we find

350   that photochemistry must be taken into account. In the case of NO_2, rapid cycling with NO (the sum of which is known as NO_x) must be considered, which varies with latitude and season. Similarly, any additional production or loss of NOx reservoir species, e.g., peroxyacyl nitrate (PAN), could significantly alter the ratio. CO is made up of direct anthropogenic and biomass burning emissions, in addition to a secondary production source from the oxidation of VOCs and methane that can contribute up to 75% of the total source in summer months. Neglecting atmospheric chemistry will compromise the ability to use these

355   tracers to determine combustion CO_2.

When investigating corresponding ratios in reported emission data, we find a weak positive relationship between $CO:CO_2$ and $NO_x:CO_2$ ratios on national levels (R<0.4), which suggests that combustion efficiency in terms of co-emitting CO and NO_x are weakly correlated within a country. We also find a weak positive correlation between emission-based ratio $CO:CO_2$ and satellite observed column enhancement $\Delta XCO:\Delta XCO_2$ (R<0.2), which suggests the consistency and linearity in CO

360 chemistry and transport. Conversely for NO_2, we find a stronger negative correlation between $NO_x:CO_2$ and enhancement $\Delta XNO_2:\Delta XCO_2$ (R<0.50), which suggests nonlinearity in NO_x photochemistry. Both of these relationships are described reasonably well (similar R values) by the atmospheric chemistry transport model, providing confidence that the model is a useful tool for interpreting these tracer-tracer ratios.

Some of the challenges we faced in our study, in particular the coincidence of TROPOMI and OCO-2 data, will be partly

365 addressed with upcoming missions that measure both NO_2 and CO_2. These missions currently include the Copernicus CO_2 Monitoring (CO2M) mission (Kuhlmann et al., 2021) and the Japanese Greenhouse Gases Observing Satellite Greenhouse gases and Water cycle (GOSAT-GW). The proposed CO2M mission is temporally staggered three-satellite constellation, resulting in better spatial coverage of the globe per day than currently provided by OCO-2. Developing virtual constellations, i.e. integrating measurements from independent missions, is an ongoing key objective but relies on rigorous calibration of data

370 collected by different sensors. Another current challenge is understanding how to use together CO_2 and reactive trace gases to infer robust combustion emission estimates of CO_2. Our work has shown that even over Europe, where our knowledge of emissions should be relatively good compared to many parts of the world, we find there are sometimes large differences between model photochemical calculations and satellite observations. Addressing this issue will need an integrated approach that draws together the atmospheric chemistry and carbon cycle communities.

Author contributions. MS and PIP designed experiments and wrote the paper. MFL and LF contributed to the processing and analysis of

380 satellite measurements. IS, SNCD and HACDvdG provided the TNO-GHGco emission inventory and advice on its usage. All co-authors helped to revise the paper.

Atmospheric
Chemistry
and Physics
Discussions

Open Access

Atmospheric
Chemistry
and Physics
Discussions

References

Abbot, D. S., Palmer, P. I., Martin, R. V., Chance, K. V., Jacob, D. J., and Guenther, A.: Seasonal and interannual variability of North American isoprene emissions as determined by formaldehyde column measurements from space, Geophysical Research Letters, 30, https://doi.org/https://doi.org/10.1029/2003GL017336, 2003.

390   Akagi, S., Yokelson, R. J., Wiedinmyer, C., Alvarado, M., Reid, J., Karl, T., Crounse, J., and Wennberg, P.: Emission factors for open and domestic biomass burning for use in atmospheric models, Atmospheric Chemistry and Physics, 11, 4039–4072, 2011.

Berezin, E., Konovalov, I., Ciais, P., Richter, A., Tao, S., Janssens-Maenhout, G., Beekmann, M., and Schulze, E.-D.: Multiannual changes of CO 2 emissions in China: indirect estimates derived from satellite measurements of tropospheric NO 2 columns, Atmospheric Chemistry and Physics, 13, 9415–9438, 2013.

395   Boersma, K., Dirksen, R., Brunner, D., Zhou, Y., Huijnen, V., Eskes, H., Veefkind, J., Kleipool, Q., Dobber, M., and Stammes, P.: An improved retrieval of tropospheric NO_2 columns from the Ozone Monitoring Instrument, Adv. Mater, 2010.

Ciais, P., Wang, Y., Andrew, R., Bréon, F. M., Chevallier, F., Broquet, G., Nabuurs, G. J., Peters, G., McGrath, M., Meng, W., Zheng, B., and Tao, S.: Biofuel burning and human respiration bias on satellite estimates of fossil fuel CO2 emissions, Environmental Research Letters, 15, 074 036, https://doi.org/10.1088/1748-9326/ab7835, 2020.

400   Crisp, D., Atlas, R., Breon, F.-M., Brown, L., Burrows, J., Ciais, P., Connor, B., Doney, S., Fung, I., Jacob, D., et al.: The orbiting carbon observatory (OCO) mission, Advances in Space Research, 34, 700–709, 2004.

Crisp, D., Rosenberg, R., Chapsky, L., Lee, R., Merrelli, A., Osterman, G., Oyafuso, F., Pollock, R., Spiers, G., Yu, S., et al.: Orbiting Carbon Observatory -2 & 3: Level 1B Algorithm Theoretical Basis, Version 2.0, rev 0, for OCO-2 v10 & 10R data and OCO-3 vEarly & EarlyR datasets, Tech. rep., NASA, Jet Propulsion Laboratory, 2021.

405   Curci, G., Palmer, P. I., Kurosu, T. P., Chance, K., and Visconti, G.: Estimating European volatile organic compound emissions using satellite observations of formaldehyde from the Ozone Monitoring Instrument, Atmospheric Chemistry and Physics, 10, 11 501–11 517, https://doi.org/10.5194/acp-10-11501-2010, 2010.

Duncan, B., Logan, J., Bey, I., Megretskaia, I., Yantosca, R., Novelli, P., Jones, N. B., and Rinsland, C.: Global budget of CO, 1988–1997: Source estimates and validation with a global model, Journal of Geophysical Research: Atmospheres, 112, 2007.

410   Eastham, S. D., Weisenstein, D. K., and Barrett, S. R.: Development and evaluation of the unified tropospheric–stratospheric chemistry extension (UCX) for the global chemistry-transport model GEOS-Chem, Atmospheric Environment, 89, 52–63, 2014.

Eldering, A., O'Dell, C. W., Wennberg, P. O., Crisp, D., Gunson, M. R., Viatte, C., Avis, C., Braverman, A., Castano, R., Chang, A., et al.: The Orbiting Carbon Observatory-2: First 18 months of science data products, Atmospheric Measurement Techniques, 10, 549–563, 2017.

Finch, D. P., Palmer, P. I., and Zhang, T.: Automated detection of atmospheric NO_2 plumes from satellite data: a tool to help infer anthro-
415   pogenic combustion emissions, Submitted to AMTD, 2021.

Fortems-Cheiney, A., Broquet, G., Pison, I., Saunois, M., Potier, E., Berchet, A., Dufour, G., Siour, G., Denier van der Gon, H., Dellaert, S. N. C., and Boersma, K. F.: Analysis of the Anthropogenic and Biogenic NOx Emissions Over 2008-2017: Assessment of the Trends in the 30 Most Populated Urban Areas in Europe, Geophysical Research Letters, 48, e2020GL092 206, https://doi.org/https://doi.org/10.1029/2020GL092206, e2020GL092206 2020GL092206, 2021a.

420   Fortems-Cheiney, A., Pison, I., Broquet, G., Dufour, G., Berchet, A., Potier, E., Coman, A., Siour, G., and Costantino, L.: Variational regional inverse modeling of reactive species emissions with PYVAR-CHIMERE-v2019, Geoscientific Model Development, 14, 2939–2957, https://doi.org/10.5194/gmd-14-2939-2021, 2021b.

Atmospheric
Chemistry
and Physics
Discussions

Fu, T.-M., Jacob, D. J., Palmer, P. I., Chance, K., Wang, Y. X., Barletta, B., Blake, D. R., Stanton, J. C., and Pilling, M. J.: Space-based formaldehyde measurements as constraints on volatile organic compound emissions in east and south Asia and implications for ozone,
425   Journal of Geophysical Research: Atmospheres, 112, https://doi.org/https://doi.org/10.1029/2006JD007853, 2007a.

Fu, T.-M., Jacob, D. J., Palmer, P. I., Chance, K., Wang, Y. X., Barletta, B., Blake, D. R., Stanton, J. C., and Pilling, M. J.: Space-based formaldehyde measurements as constraints on volatile organic compound emissions in east and south Asia and implications for ozone, Journal of Geophysical Research: Atmospheres, 112, https://doi.org/https://doi.org/10.1029/2006JD007853, 2007b.

Gonzi, S., Palmer, P. I., Barkley, M. P., De Smedt, I., and Van Roozendael, M.: Biomass burning emission estimates inferred from
430   satellite column measurements of HCHO: Sensitivity to co-emitted aerosol and injection height, Geophysical Research Letters, 38, https://doi.org/https://doi.org/10.1029/2011GL047890, 2011.

Griffin, D., Zhao, X., McLinden, C. A., Boersma, F., Bourassa, A., Dammers, E., Degenstein, D., Eskes, H., Fehr, L., Fioletov, V., et al.: High-resolution mapping of nitrogen dioxide with TROPOMI: First results and validation over the Canadian oil sands, Geophysical Research Letters, 46, 1049–1060, 2019.

435 Hakkarainen, J., Ialongo, I., Maksyutov, S., and Crisp, D.: Analysis of four years of global XCO2 anomalies as seen by orbiting carbon observatory-2, Remote Sensing, 11, 850, 2019.

Hakkarainen, J., Szeląg, M. E., Ialongo, I., Retscher, C., Oda, T., and Crisp, D.: Analyzing nitrogen oxides to carbon dioxide emission ratios from space: A case study of Matimba Power Station in South Africa, Atmospheric Environment: X, 10, 100 110, https://doi.org/10.1016/j.aeaoa.2021.100110, 2021.

440 Hoesly, R. M., Smith, S. J., Feng, L., Klimont, Z., Janssens-Maenhout, G., Pitkanen, T., Seibert, J. J., Vu, L., Andres, R. J., Bolt, R. M., et al.: Historical (1750–2014) anthropogenic emissions of reactive gases and aerosols from the Community Emissions Data System (CEDS), Geoscientific Model Development, 11, 369–408, 2018.

Ialongo, I., Stepanova, N., Hakkarainen, J., Virta, H., and Gritsenko, D.: Satellite-based estimates of nitrogen oxide and methane emissions from gas flaring and oil production activities in Sakha Republic, Russia, Atmospheric Environment: X, 11, 100 114,
445   https://doi.org/10.1016/j.aeaoa.2021.100114, 2021.

Kasibhatla, P., Arellano, A., Logan, J. A., Palmer, P. I., and Novelli, P.: Top-down estimate of a large source of atmospheric carbon monoxide associated with fuel combustion in Asia, Geophysical Research Letters, 29, 6–1–6–4, https://doi.org/https://doi.org/10.1029/2002GL015581, 2002.

Konovalov, I. B., Berezin, E. V., Ciais, P., Broquet, G., Beekmann, M., Hadji-Lazaro, J., Clerbaux, C., Andreae, M. O., Kaiser, J. W., and
450   Schulze, E.-D.: Constraining CO2 emissions from open biomass burning by satellite observations of co-emitted species: a method and its application to wildfires in Siberia, Atmospheric Chemistry and Physics, 14, 10 383–10 410, https://doi.org/10.5194/acp-14-10383-2014, 2014.

Konovalov, I. B., Berezin, E. V., Ciais, P., Broquet, G., Zhuravlev, R. V., and Janssens-Maenhout, G.: Estimation of fossil-fuel CO2 emissions using satellite
455 measurements of "proxy" species, Atmospheric Chemistry and Physics, 16, 13 509–13 540, https://doi.org/10.5194/acp-16-13509-2016, 2016.

Kuhlmann, G., Henne, S., Meijer, Y., and Brunner, D.: Quantifying CO2 Emissions of Power Plants With CO2 and NO2 Imaging Satellites, Frontiers in Remote Sensing, 2, 14, https://doi.org/10.3389/frsen.2021.689838, 2021.

Labzovskii, L. D., Jeong, S.-J., and Parazoo, N. C.: Working towards confident spaceborne monitoring of carbon emissions from cities using
460   Orbiting Carbon Observatory-2, Remote Sensing of Environment, 233, 111 359, 2019.

15

Lama, S., Houweling, S., Boersma, K. F., Eskes, H., Aben, I., Denier van der Gon, H. A., Krol, M. C., Dolman, H., Borsdorff, T., and Lorente, A.: Quantifying burning efficiency in megacities using the NO 2/ CO ratio from the Tropospheric Monitoring Instrument (TROPOMI), Atmospheric Chemistry and Physics, 20, 10 295–10 310, 2020.

465   Landgraf, J., Scheepmaker, R., Borsdorff, T., Hu, H., Houweling, S., Butz, A., Aben, I., Hasekamp, O., et al.: Carbon monoxide total column retrievals from TROPOMI shortwave infrared measurements, Atmospheric Measurement Techniques, 9, 4955–4975, 2016.

Laughner, J. L. and Cohen, R. C.: Direct observation of changing NOx lifetime in North American cities, Science, 366, 723–727, https://doi.org/10.1126/science.aax6832, 2019.

Laughner, J. L., Zare, A., and Cohen, R. C.: Effects of daily meteorology on the interpretation of space-based remote sensing of NO 2, Atmospheric Chemistry and Physics, 16, 15 247–15 264, 2016.

470   Liu, F., Duncan, B. N., Krotkov, N. A., Lamsal, L. N., Beirle, S., Griffin, D., McLinden, C. A., Goldberg, D. L., and Lu, Z.: A methodology to constrain carbon dioxide emissions from coal-fired power plants using satellite observations of co-emitted nitrogen dioxide, Atmospheric Chemistry and Physics, 20, 99–116, https://doi.org/10.5194/acp-20-99-2020, 2020.

Lorente, A., Folkert Boersma, K., Yu, H., Dörner, S., Hilboll, A., Richter, A., Liu, M., Lamsal, L. N., Barkley, M., Smedt, I. D., et al.: Structural uncertainty in air mass factor calculation for NO$_2$ and HCHO satellite retrievals, Atmospheric Measurement Techniques, 10,
475   759–782, 2017.

O'dell, C. W., Eldering, A., Wennberg, P. O., Crisp, D., Gunson, M. R., Fisher, B., Frankenberg, C., Kiel, M., Lindqvist, H., Mandrake, L., et al.: Improved retrievals of carbon dioxide from Orbiting Carbon Observatory-2 with the version 8 ACOS algorithm, Atmospheric Measurement Techniques, 11, 6539–6576, 2018.

Palmer, P. I., Jacob, D. J., Fiore, A. M., Martin, R. V., Chance, K., and Kurosu, T. P.: Mapping isoprene emissions over
480   North America using formaldehyde column observations from space, Journal of Geophysical Research: Atmospheres, 108, https://doi.org/https://doi.org/10.1029/2002JD002153, 2003.

Palmer, P. I., Abbot, D. S., Fu, T.-M., Jacob, D. J., Chance, K., Kurosu, T. P., Guenther, A., Wiedinmyer, C., Stanton, J. C., Pilling, M. J., Pressley, S. N., Lamb, B., and Sumner, A. L.: Quantifying the seasonal and interannual variability of North American isoprene emissions using satellite observations of the formaldehyde column, Journal of Geophysical Research: Atmospheres, 111,
485   https://doi.org/https://doi.org/10.1029/2005JD006689, 2006.

Park, H., Jeong, S., Park, H., Labzovskii, L. D., and Bowman, K. W.: An assessment of emission characteristics of Northern Hemisphere cities using spaceborne observations of CO2, CO, and NO2, Remote Sensing of Environment, 254, 112 246, 2021.

Platt, U. and Stutz, J.: Differential absorption spectroscopy, in: Differential Optical Absorption Spectroscopy, pp. 135–174, Springer, 2008.

Pope, R. J., Arnold, S. R., Chipperfield, M. P., Latter, B. G., Siddans, R., and Kerridge, B. J.: Widespread changes in UK air quality observed
490   from space, Atmospheric Science Letters, 19, e817, 2018.

Reuter, M., Buchwitz, M., Schneising, O., Krautwurst, S., O'Dell, C. W., Richter, A., Bovensmann, H., and Burrows, J. P.: Towards monitoring localized CO2 emissions from space: co-located regional CO2 and NO2 enhancements observed by the OCO-2 and S5P satellite, Atmospheric Chemistry and Physics, 19, 9371–9383, https://doi.org/10.5194/acp-19-9371-2019, 2019.

Silva, S. J. and Arellano, A.: Characterizing regional-scale combustion using satellite retrievals of CO, NO2 and CO2, Remote Sensing, 9,
495   744, 2017.

Silva, S. J., Arellano, A. F., and Worden, H. M.: Toward anthropogenic combustion emission constraints from space-based analysis of urban CO2/CO sensitivity, Geophysical Research Letters, 40, 4971–4976, 2013.

Smedt, I. D., Theys, N., Yu, H., Danckaert, T., Lerot, C., Compernolle, S., Roozendael, M. V., Richter, A., Hilboll, A., Peters, E., et al.: Algorinthm theoretical baseline for formaldehyde retrievals from S5P TROPOMI and from the QA4ECV project, Atmospheric Measurement Techniques, 11, 2395–2426, 2018.

Super, I., Dellaert, S. N., Visschedijk, A. J., and Denier van der Gon, H. A.: Uncertainty analysis of a European high-resolution emission inventory of CO_2 and CO to support inverse modelling and network design, Atmospheric Chemistry and Physics, 20, 1795–1816, 2020.

Surl, L., Palmer, P. I., and González Abad, G.: Which processes drive observed variations of HCHO columns over India?, Atmospheric Chemistry and Physics, 18, 4549–4566, https://doi.org/10.5194/acp-18-4549-2018, 2018.

Van Geffen, J., Boersma, K., Van Roozendael, M., Hendrick, F., Mahieu, E., De Smedt, I., Sneep, M., and Veefkind, J.: Improved spectral fitting of nitrogen dioxide from OMI in the 405–465 nm window, Atmospheric Measurement Techniques, 8, 1685–1699, 2015.

Van Geffen, J., Boersma, K. F., Eskes, H., Sneep, M., Ter Linden, M., Zara, M., and Veefkind, J. P.: S5P TROPOMI NO2 slant column retrieval: method, stability, uncertainties and comparisons with OMI, Atmospheric Measurement Techniques, 13, 1315–1335, 2020.

van Marle, M. J., Field, R. D., van der Werf, G. R., de Wagt, I. A. E., Houghton, R. A., Rizzo, L. V., Artaxo, P., and Tsigaridis, K.: Fire and deforestation dynamics in Amazonia (1973–2014), Global biogeochemical cycles, 31, 24–38, 2017.

Veefkind, J., Aben, I., McMullan, K., Förster, H., De Vries, J., Otter, G., Claas, J., Eskes, H., De Haan, J., Kleipool, Q., et al.: TROPOMI on the ESA Sentinel-5 Precursor: A GMES mission for global observations of the atmospheric composition for climate, air quality and ozone layer applications, Remote sensing of environment, 120, 70–83, 2012.

Vidot, J., Landgraf, J., Hasekamp, O., Butz, A., Galli, A., Tol, P., and Aben, I.: Carbon monoxide from shortwave infrared reflectance measurements: A new retrieval approach for clear sky and partially cloudy atmospheres, Remote sensing of environment, 120, 255–266, 2012.

Wang, H., Jacob, D. J., Kopacz, M., Jones, D. B. A., Suntharalingam, P., Fisher, J. A., Nassar, R., Pawson, S., and Nielsen, J. E.: Error correlation between CO_2 and CO as constraint for CO_2 flux inversions using satellite data, Atmospheric Chemistry and Physics, 9, 7313–7323, https://doi.org/10.5194/acp-9-7313-2009, 2009.

Weng, H., Lin, J., Martin, R., Millet, D. B., Jaeglé, L., Ridley, D., Keller, C., Li, C., Du, M., and Meng, J.: Global high-resolution emissions of soil NO x, sea salt aerosols, and biogenic volatile organic compounds, Scientific Data, 7, 1–15, 2020.

Zara, M., Boersma, K. F., Smedt, I. D., Richter, A., Peters, E., Van Geffen, J. H., Beirle, S., Wagner, T., Roozendael, M. V., Marchenko, S., et al.: Improved slant column density retrieval of nitrogen dioxide and formaldehyde for OMI and GOME-2A from QA4ECV: intercomparison, uncertainty characterisation, and trends, Atmospheric Measurement Techniques, 11, 4033–4058, 2018.
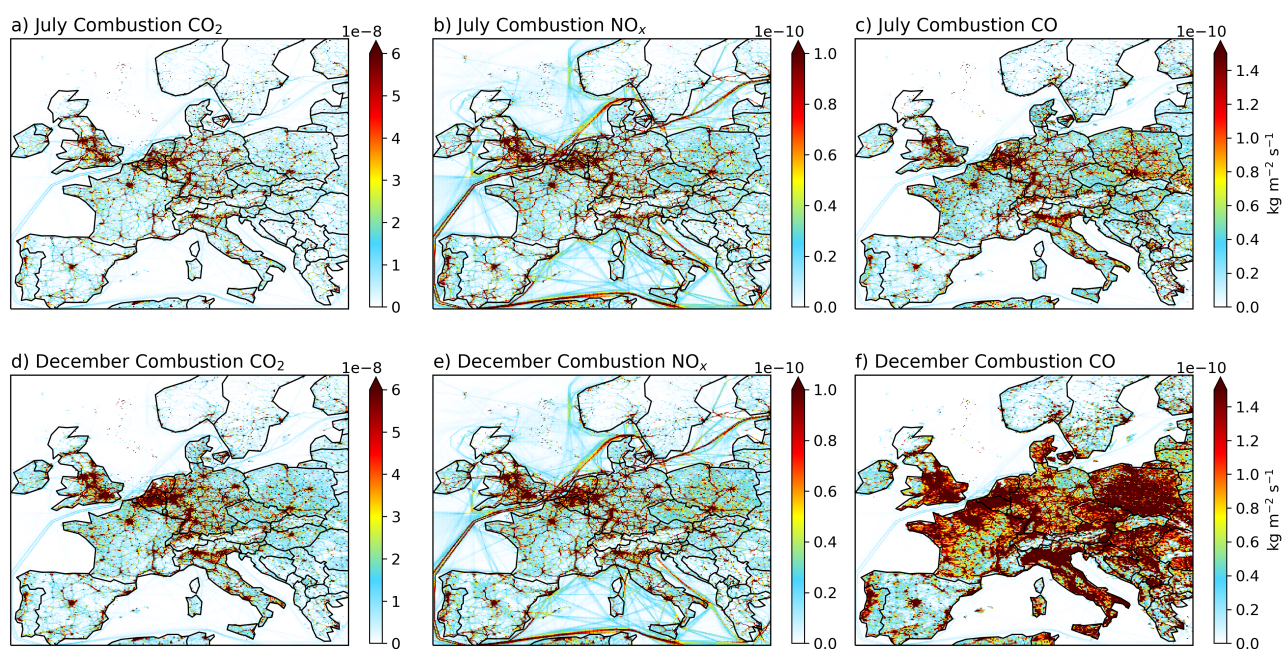
Figure 1. Combustion emissions of (left columns) CO_2, (middle columns) NO_x, and (right columns) CO (kg m^{-2} s^{-1}) over our European study domain from the TNO-GHGco inventory during (top row) July and (bottom row) December, 2018, described on the original 0.05° latitude × 0.1° longitude horizontal resolution.
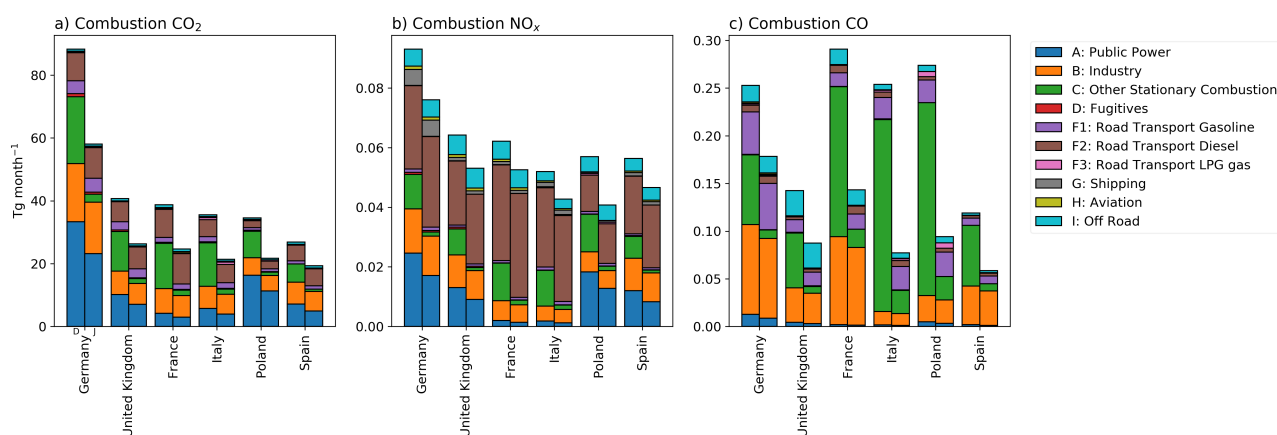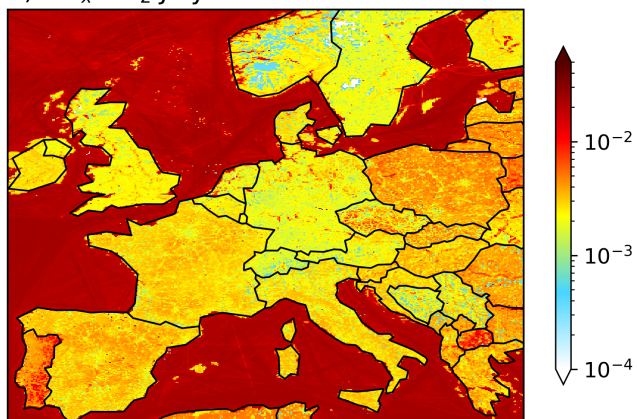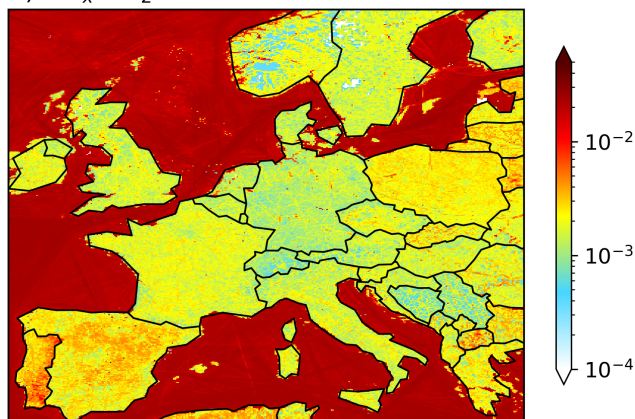
Figure 2. Sector contributions to national total combustion emissions (Tg month^{-1}) of CO_2, NO_x and CO for the top six CO_2 emitting countries across our European study domain. The two columns reported for each country denote values for (left) December and (right) July, 2018.
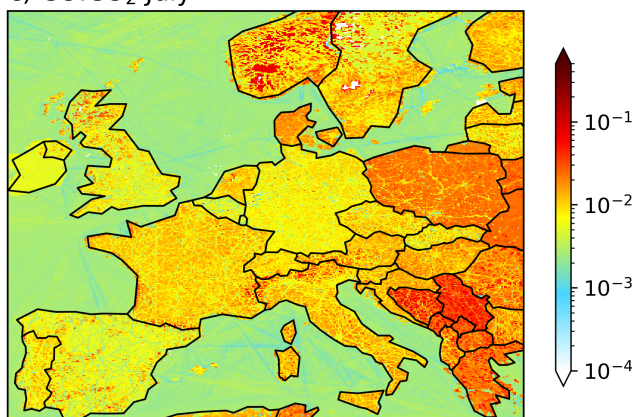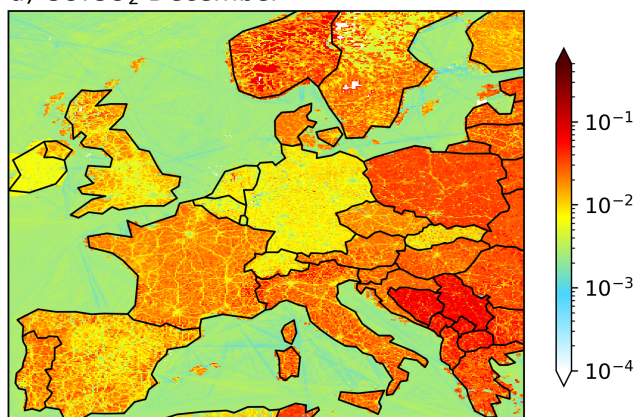
Figure 3. Spatially distribution of combustion emission mole ratios (mole/mole) of (top row) NO_x:CO_2 and (bottom row) CO:CO_2 from the TNO-GHGco inventory during (left column) July and (right column) December 2018, described on the original 0.05° latitude × 0.1° longitude horizontal resolution.
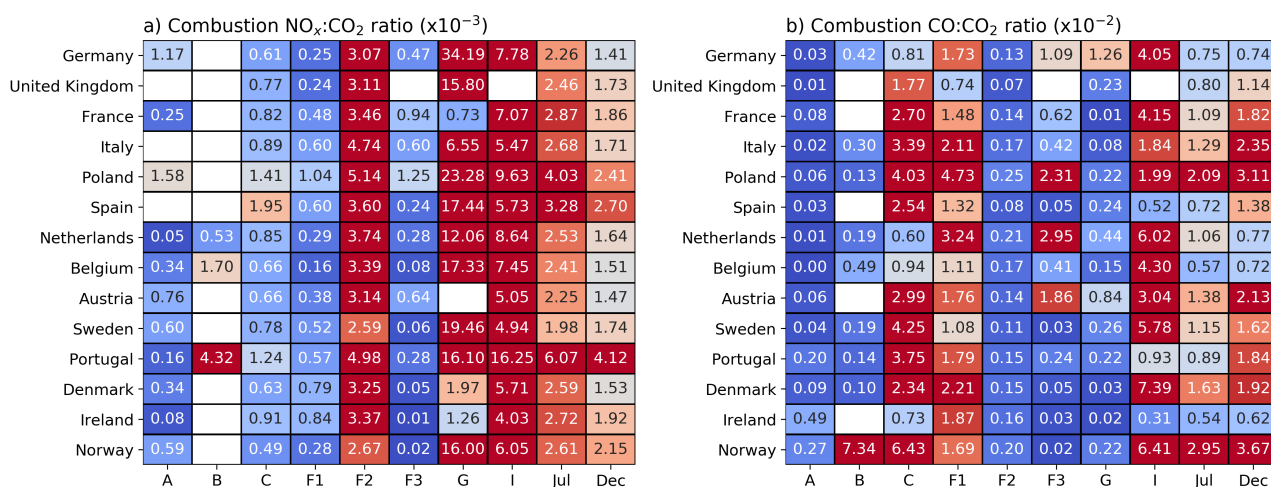
a) Combustion NO_x:CO_2 ratio ($\times 10^{-3}$)

	A	B	C	F1	F2	F3	G	I	Jul	Dec
Germany	1.17		0.61	0.25	3.07	0.47	34.19	7.78	2.26	1.41
United Kingdom			0.77	0.24	3.11		15.80		2.46	1.73
France	0.25		0.82	0.48	3.46	0.94	0.73	7.07	2.87	1.86
Italy			0.89	0.60	4.74	0.60	6.55	5.47	2.68	1.71
Poland	1.58		1.41	1.04	5.14	1.25	23.28	9.63	4.03	2.41
Spain			1.95	0.60	3.60	0.24	17.44	5.73	3.28	2.70
Netherlands	0.05	0.53	0.85	0.29	3.74	0.28	12.06	8.64	2.53	1.64
Belgium	0.34	1.70	0.66	0.16	3.39	0.08	17.33	7.45	2.41	1.51
Austria	0.76		0.66	0.38	3.14	0.64		5.05	2.25	1.47
Sweden	0.60		0.78	0.52	2.59	0.06	19.46	4.94	1.98	1.74
Portugal	0.16	4.32	1.24	0.57	4.98	0.28	16.10	16.25	6.07	4.12
Denmark	0.34		0.63	0.79	3.25	0.05	1.97	5.71	2.59	1.53
Ireland	0.08		0.91	0.84	3.37	0.01	1.26	4.03	2.72	1.92
Norway	0.59		0.49	0.28	2.67	0.02	16.00	6.05	2.61	2.15

b) Combustion CO:CO_2 ratio ($\times 10^{-2}$)

	A	B	C	F1	F2	F3	G	I	Jul	Dec
Germany	0.03	0.42	0.81	1.73	0.13	1.09	1.26	4.05	0.75	0.74
United Kingdom	0.01		1.77	0.74	0.07		0.23		0.80	1.14
France	0.08		2.70	1.48	0.14	0.62	0.01	4.15	1.09	1.82
Italy	0.02	0.30	3.39	2.11	0.17	0.42	0.08	1.84	1.29	2.35
Poland	0.06	0.13	4.03	4.73	0.25	2.31	0.22	1.99	2.09	3.11
Spain	0.03		2.54	1.32	0.08	0.05	0.24	0.52	0.72	1.38
Netherlands	0.01	0.19	0.60	3.24	0.21	2.95	0.44	6.02	1.06	0.77
Belgium	0.00	0.49	0.94	1.11	0.17	0.41	0.15	4.30	0.57	0.72
Austria	0.06		2.99	1.76	0.14	1.86	0.84	3.04	1.38	2.13
Sweden	0.04	0.19	4.25	1.08	0.11	0.03	0.26	5.78	1.15	1.62
Portugal	0.20	0.14	3.75	1.79	0.15	0.24	0.22	0.93	0.89	1.84
Denmark	0.09	0.10	2.34	2.21	0.15	0.05	0.03	7.39	1.63	1.92
Ireland	0.49		0.73	1.87	0.16	0.03	0.02	0.31	0.54	0.62
Norway	0.27	7.34	6.43	1.69	0.20	0.02	0.22	6.41	2.95	3.67

Figure 4. Heatmap of national-scale combustion emission mole ratios (mole/mole) for (a) NO_x:CO_2 and (b) CO:CO_2 from eight major sectors in the top 14 CO_2 emitting countries: A: Public Power; B: Industry; C: Other Stationary Combustion; F1: Road Transport Gasoline; F2: Road Transport Diesel; F3: Road Transport LPG Gas; G: Shipping; and I: Off Road) and two contrasting months (July and December). Sector D - Fugitve and H - Aviation are excluded due to relatively smaller contribution to the total combustion emission in the domain.
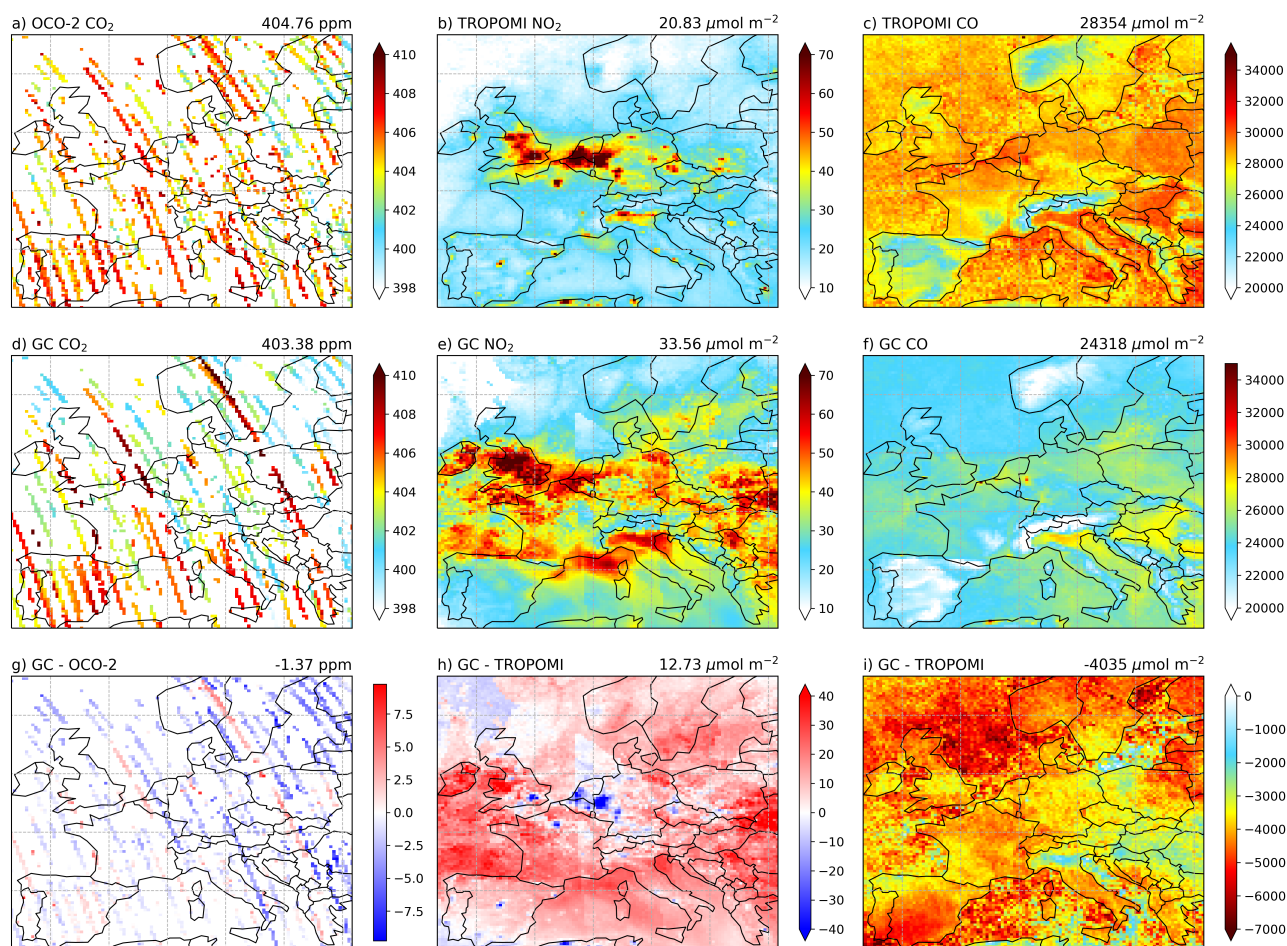
Figure 5. Satellite measurements and GEOS-Chem model columns of CO_2 (ppm), CO ($\mu\,mol\;m^{-2}$), NO_2 ($\mu\,mol\;m^{-2}$), described on 0.25° latitude × 0.3125° longitude resolution. The top row shows observed distributions from OCO-2 and TROPOMI, the middle row shows the corresponding GEOS-Chem distributions, and the bottom row shows GEOS-Chem minus observed distributions. Domain-mean values and units are shown in the titles of each panel.
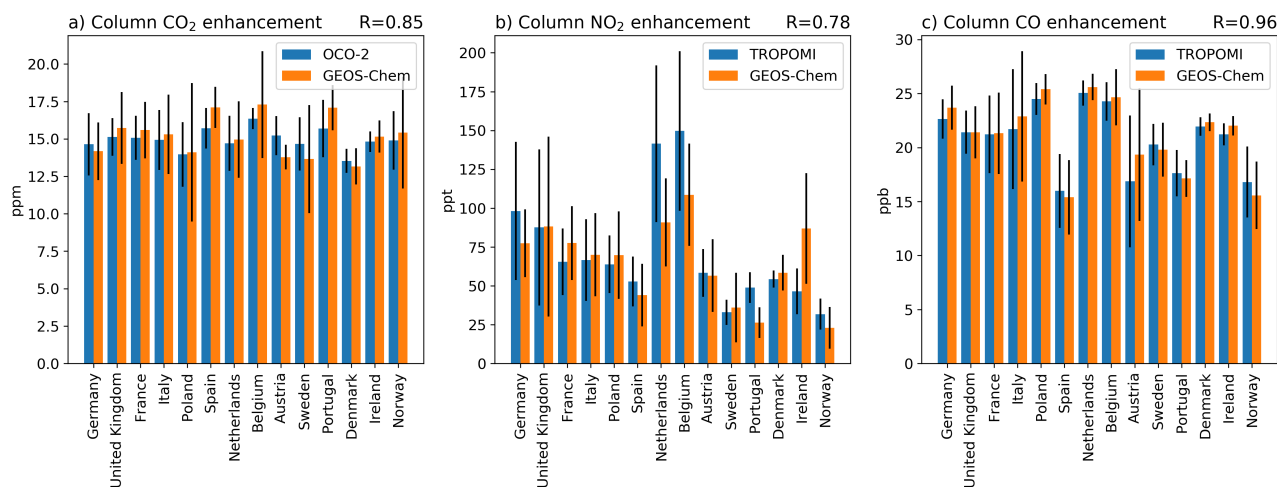
Atmospheric
Chemistry
and Physics
Discussions

Figure 6. Observed and GEOS-Chem monthly mean and standard deviation of (a) ΔXCO_2 (ppm), and (b) ΔNO_2 (ppt) and (c) ΔCO columns (ppb) during July 2018 for the top 14 CO_2 emitting countries, in descending order. Correlation coefficients from linear regression are shown on sub-panel title.
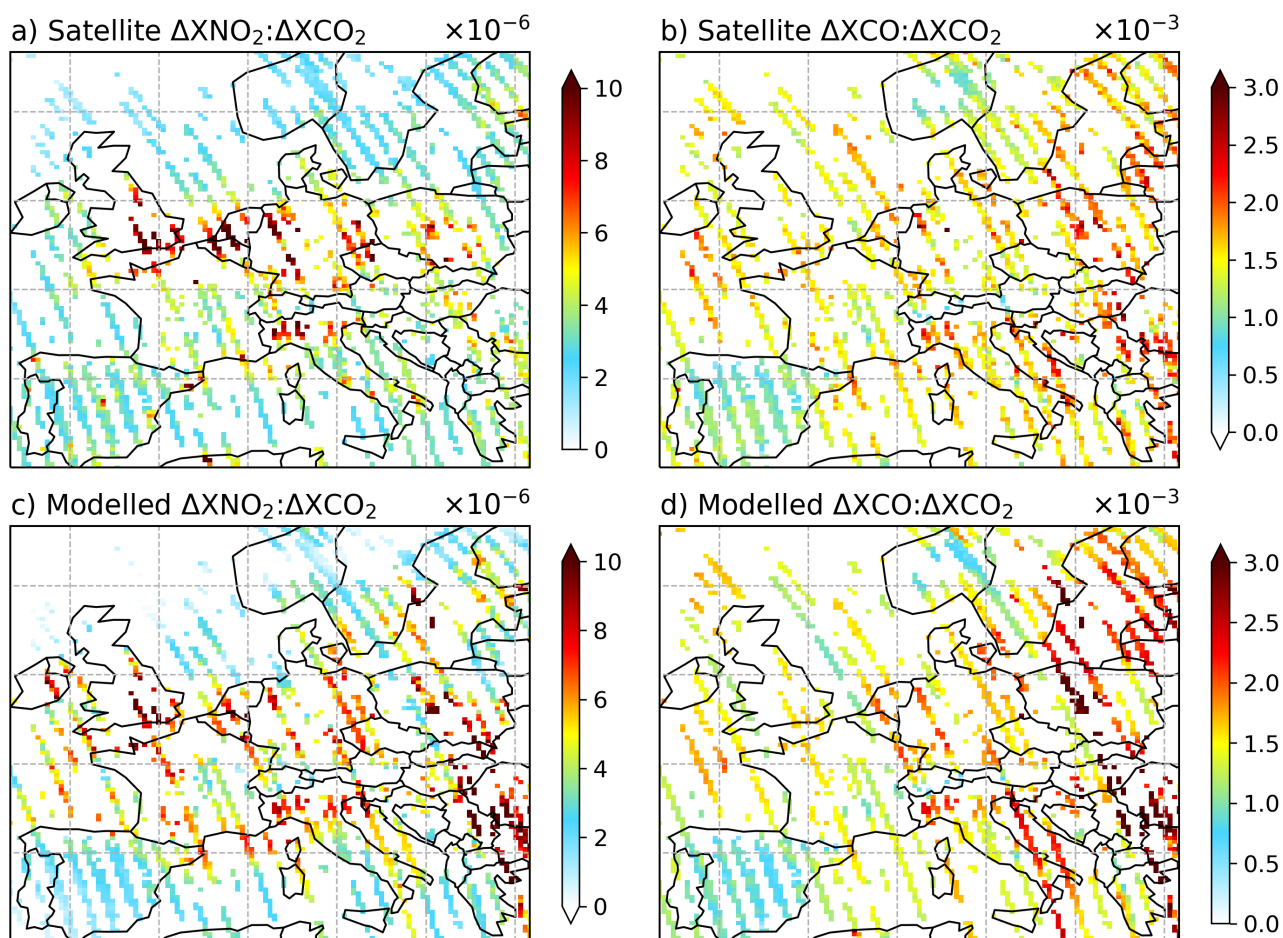
Figure 7. Observed and GEOS-Chem monthly mean European distributions of (left) ΔXNO_2:ΔXCO_2 and (right) ΔXCO:ΔXCO_2 ratios during July 2018, described on 0.25° latitude × 0.3125° longitude resolution.
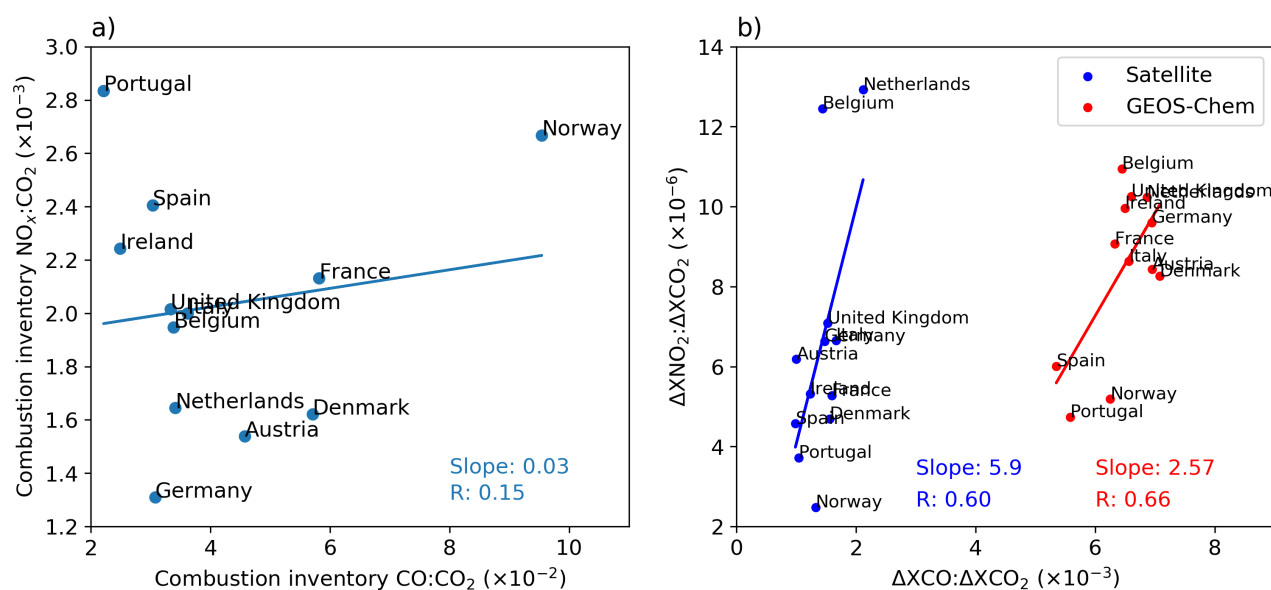
Figure 8. European country relationships of a) emission inventory ratios of $CO:CO_2$ and $NO_x:CO_2$ and b) (blue) observed and (red) GEOS-Chem ratios of $\Delta XNO_2:\Delta XCO_2$ during July 2018. Correlation coefficients and slopes from linear regression are shown inset of each panel.
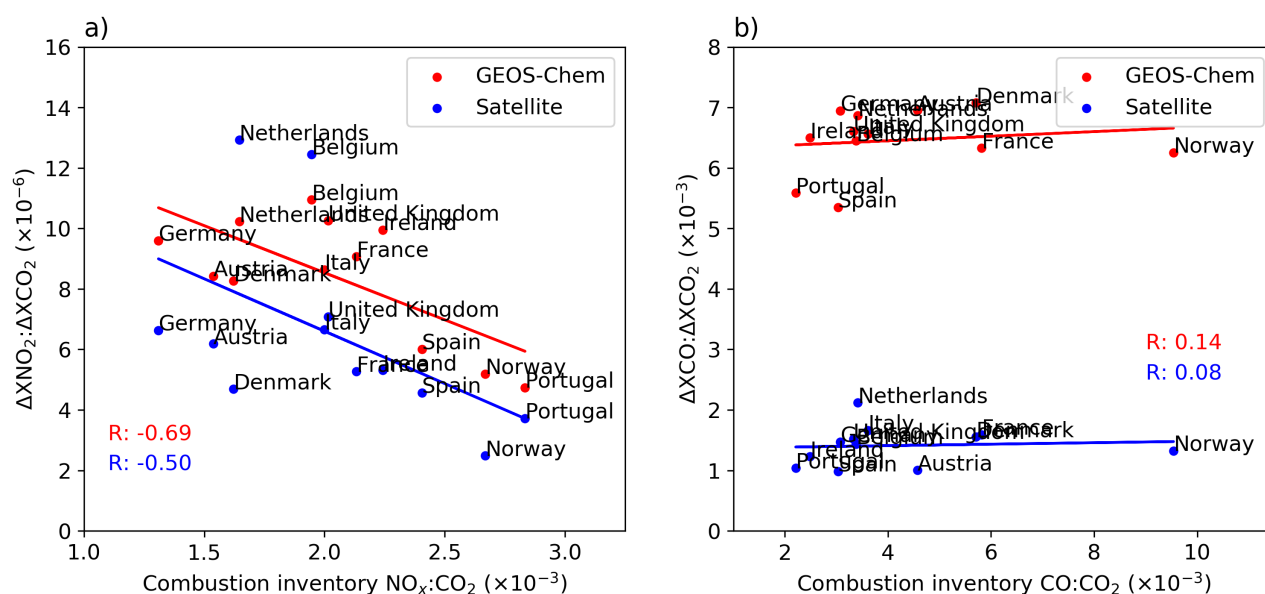
Figure 9. European country relationships of inventory estimates of combustion $NO_x:CO_2$ and $CO:CO_2$ and observed and GEOS-Chem atmospheric ratios of $\Delta XNO_2:\Delta XCO_2$ and $\Delta XCO:\Delta XCO_2$. Correlation coefficients and slopes from linear regression are shown inset of each panel.

Atmospheric
Chemistry
and Physics
Discussions

Open Access

EGU
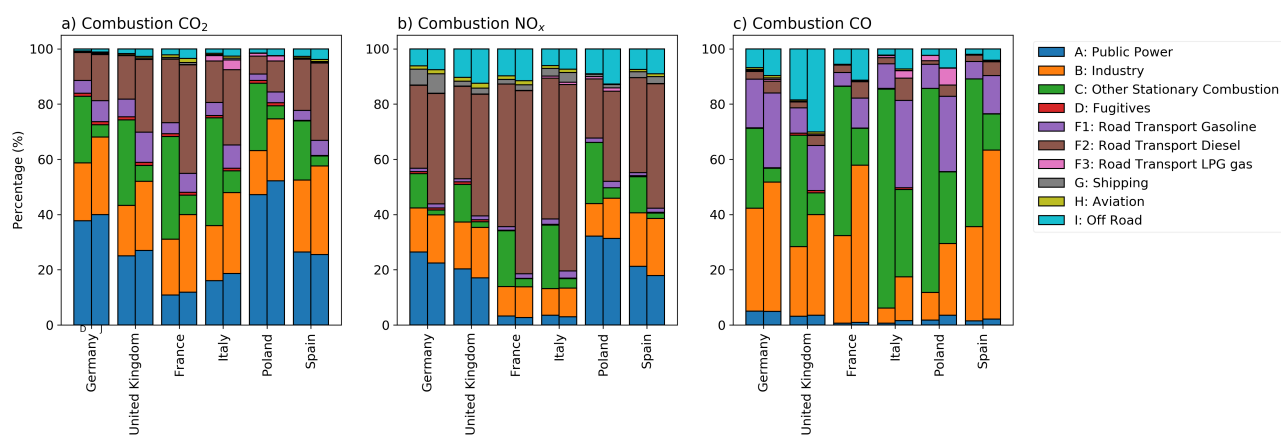
Figure A1. Sector percentage contribution to national total combustion emission of CO_2, NO_x and CO in (left) December and (right) July 2018 for six European countries.

Atmospheric
Chemistry
and Physics
Discussions
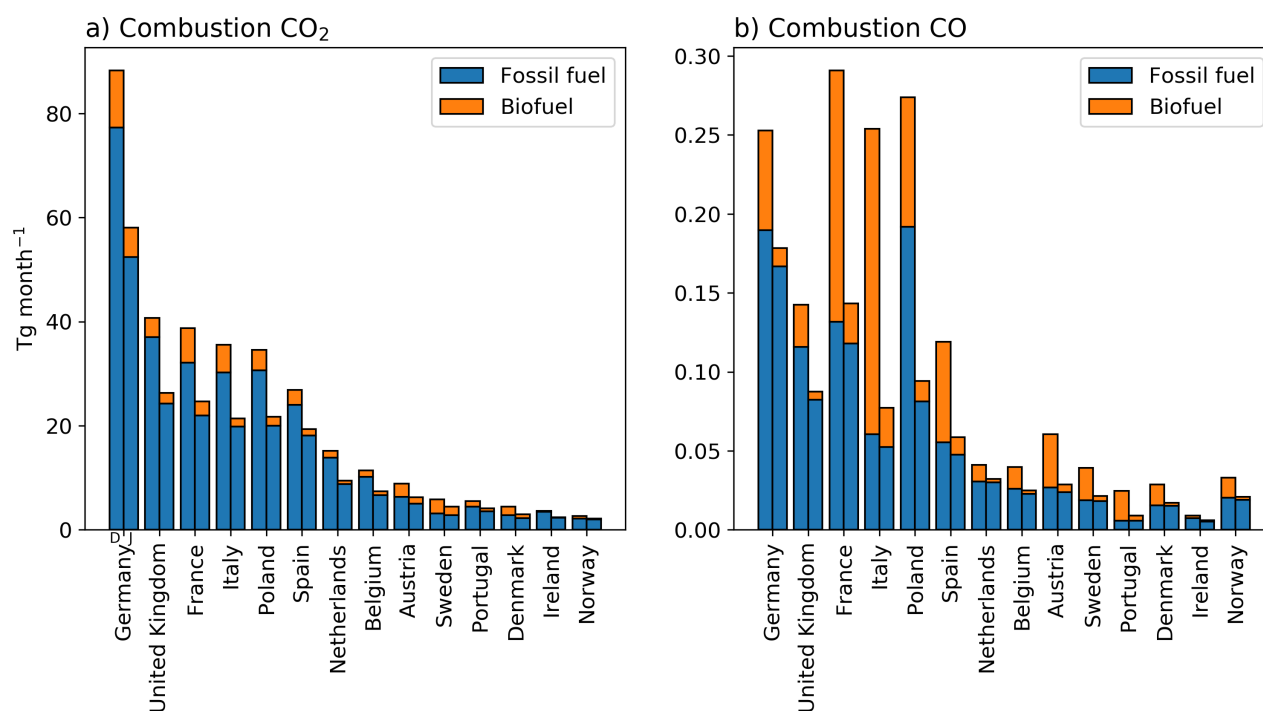
Figure A2. Fuel type contribution to national total combustion emissions (Tg month^{-1}) of CO_2 and CO in (left) December and (right) July 2018 for 14 European countries.
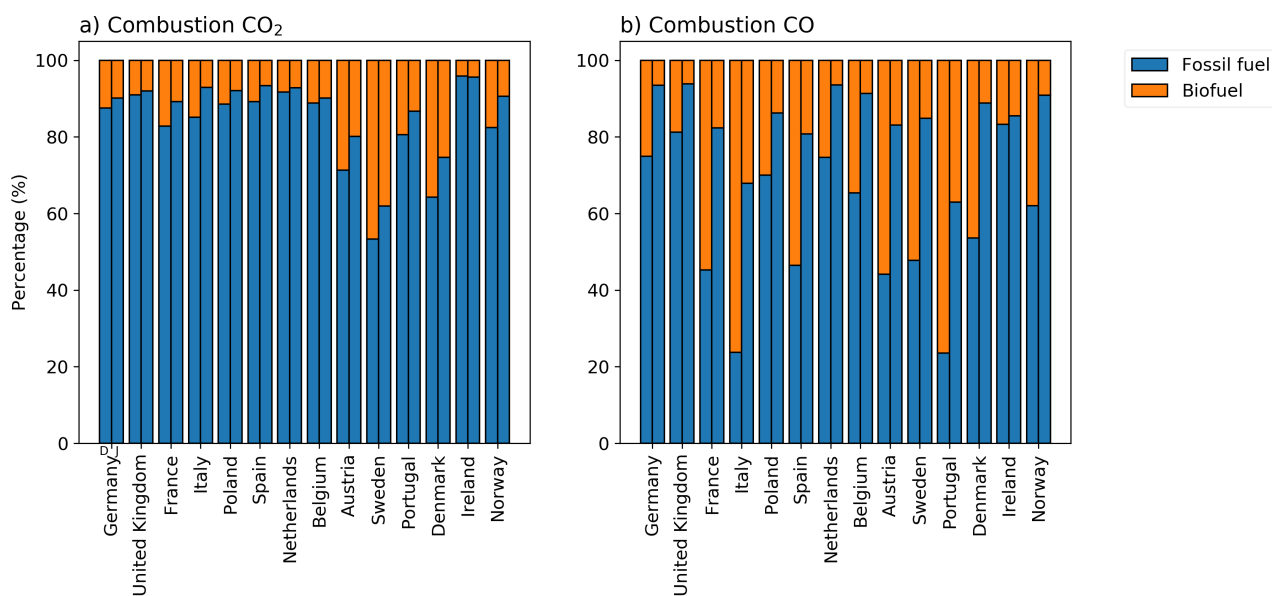
Figure A3. Fuel type percentage contribution to national total combustion emission of CO_2 and CO in (left) December and (right) July 2018 for 14 European countries.
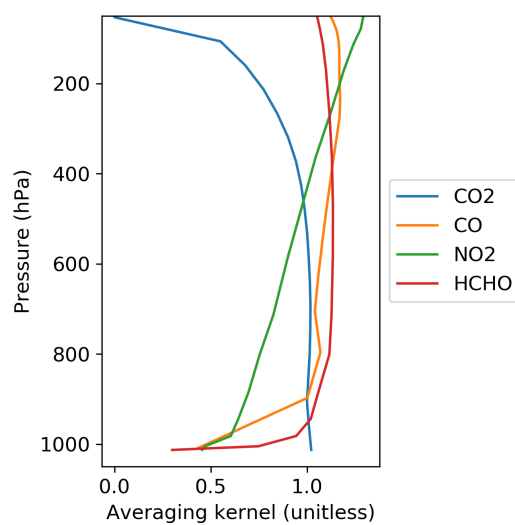
Figure A4. Example averaging kernels of NO_2, CO, HCHO from TROPOMI and CO_2 from OCO-2, on July 5th, 2018 over London, UK.
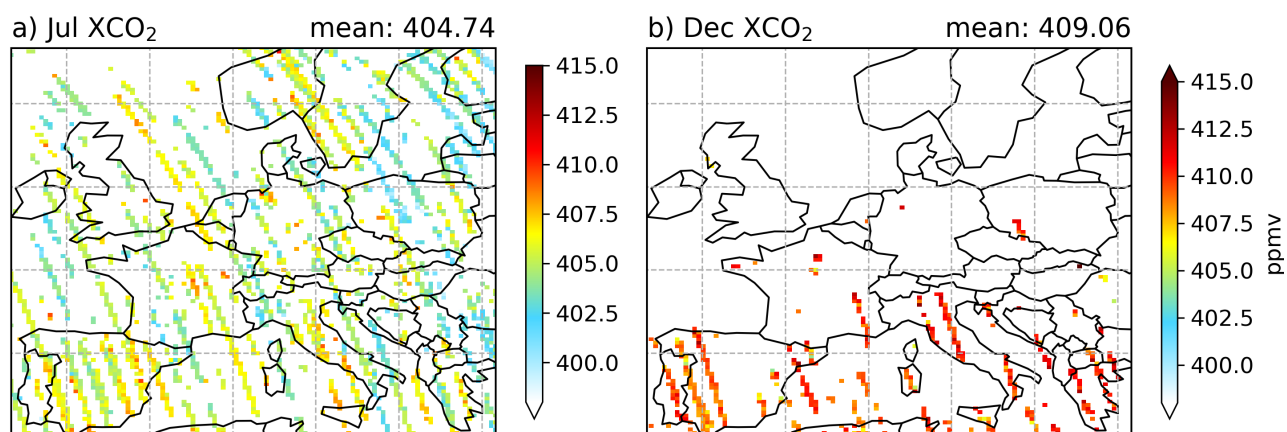
Figure A5. Monthly mean dry air column concentration of CO_2 (XCO_2) retrieved by OCO-2 during (left) July and (right) December 2018. Values are gridded on the GEOS-Chem model spatial resolution of $0.25°$(latitude) $\times$ $0.3125°$(longitude).
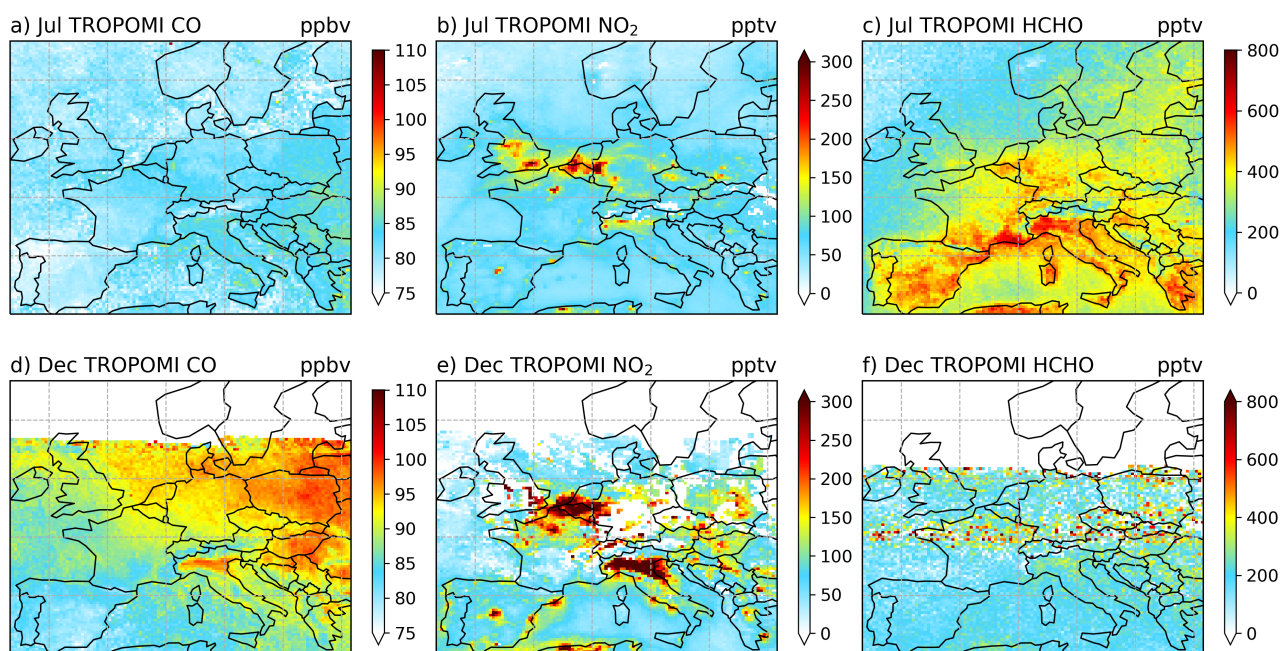
Figure A6. Monthly mean column density of CO, NO$_2$ and HCHO observed by TROPOMI in (top row) July and (bottom row) December 2018, only data points with qa$_{value}$ > 0.75 are selected. Values are gridded on the GEOS-Chem model spatial resolution of 0.25° (latitude) × 0.3125° (longitude).

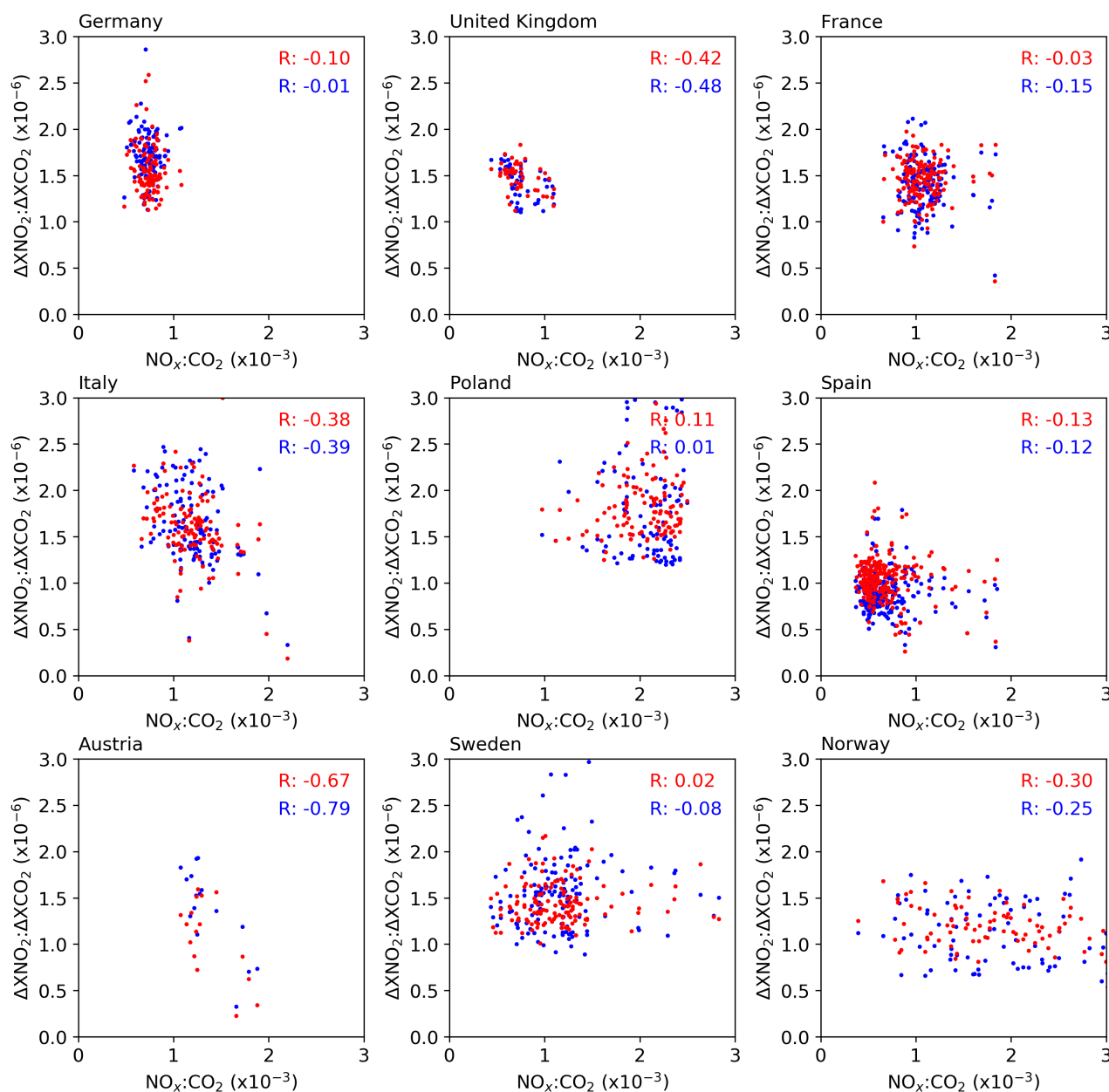**Figure A7.** Relationship between combustion emission NO_x:CO_2 and satellite measured ΔXNO_2:ΔXCO_2 (blue) and GEOS-Chem simulated ΔXNO_2:ΔXCO_2 (red) for nine European countries. Correlation coefficient value of simple linear regression analysis is shown on the sub-panel figure.
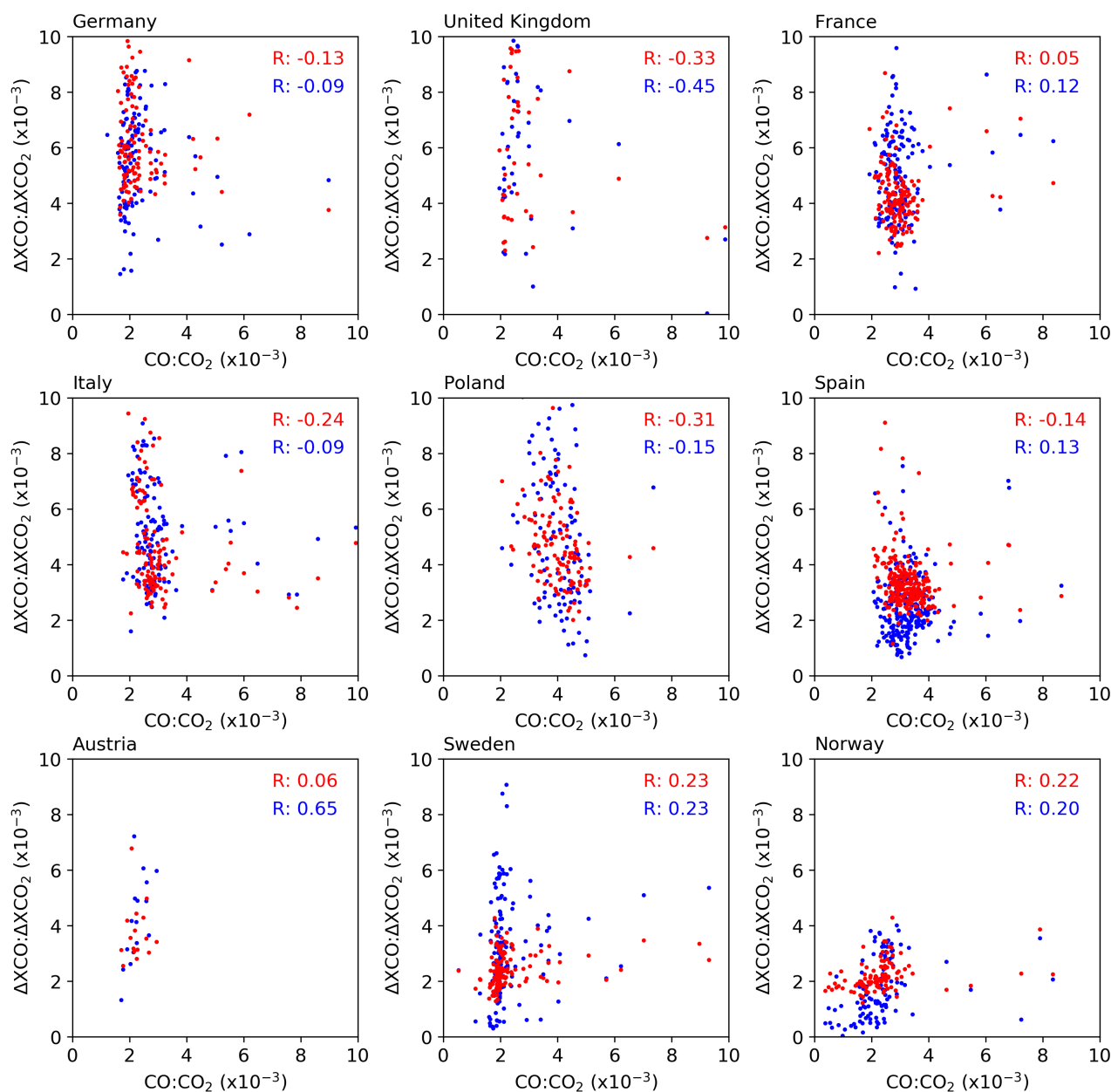
Figure A8. Relationship between combustion emission $CO:CO_2$ and satellite measured $\Delta XCO:\Delta XCO_2$ (blue) and GEOS-Chem simulated $\Delta XCO:\Delta XCO_2$ (red) for nine European countries. Correlation coefficient value of simple linear regression analysis is shown on the sub-panel figure.